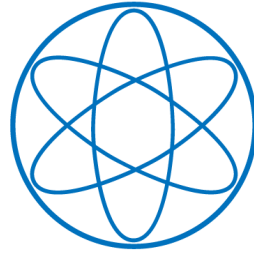


LEHRSTUHL E15
PHYSIK - DEPARTMENT



**Spectral Analysis of Neutrino and
Background Events in the solar
Neutrino Experiments BOREXINO
and LENA**

DIPLOMA THESIS

FELICITAS ANDREA THORNE
1ST OF DECEMBER 2010



TECHNISCHE UNIVERSITÄT MÜNCHEN

Abstract

The solar neutrino experiment BOREXINO, is a 300 t liquid scintillator detector, located at the Laboratori Nazionali del Gran Sasso (LNGS) in Italy. It is the first experiment which is able to measure solar neutrinos in the sub-MeV range in real-time. The neutrino signal is detected via neutrino-electron scattering which cannot be extracted from the experimental data by coincidence analysis. Therefore, the event rates of the different solar neutrino sources have to be determined by spectral analyses. While some background (muons, cosmogenic background, fast coincidences) can be tagged event-by-event, most background originating from β decays cannot be distinguished from neutrino-electron scattering. Thus, electron recoil spectra from neutrino events and β spectra from background sources have to be fitted simultaneously.

After starting the data taking in May 2007, it took the BOREXINO collaboration only three months to publish the first real-time measurement of solar ${}^7\text{Be}$ neutrinos with an event rate of $47 \pm 7_{\text{stat}} \pm 12_{\text{sys}}$ cpd/100t. In 2008, BOREXINO also observed the solar ${}^8\text{B}$ neutrinos and their flux was determined to $\Phi_{\text{sB}} = 2.4 \pm 0.4 \pm 0.1 \cdot 10^6 \text{cm}^{-2}\text{s}^{-1}$. Encouraged by this result, the collaboration set one of the next goals to be the detection of solar pep and CNO neutrinos, which would provide crucial information on the MSW effect and the metallicity of the Sun.

The main part of this thesis is focused on the detection of pep neutrinos in BOREXINO by spectral analysis. Therefore, a procedure for performing this analysis was developed based on the theory of β decays and neutrino-electron scattering including the quenching effects and the energy resolution of the detector. This tool was tested on Monte Carlo data and experimental data before it has been applied on a BOREXINO data sample with 633.82 days of detector life time. The spectral fit results in a pep neutrino event rate of $2.66 \pm 1.04(\text{stat}) \pm 0.30(\text{sys})$ cpd/100t with a statistical significance of 99.998%. In addition, an upper limit of 0.78 cpd/100t at a 95% confidence level could be set on the event rate of the primordial isotope ${}^{40}\text{K}$ in BOREXINO, by including its spectral shape to the analysis.

Furthermore, the application of spectral fits on data from neutrino oscillometry in LENA (Low Energy Neutrino Astronomy), a proposed next-generation neutrino experiment based on a 50kt target of liquid scintillator, is investigated with regard to a measurement of the still unknown neutrino mixing angle θ_{13} .

Contents

1	Neutrino characteristics and the Standard Solar Model	1
1.1	The Standard Model of particle physics	1
1.2	Characteristics of neutrinos	3
1.2.1	Neutrino oscillations in vacuum	4
1.2.2	Neutrino oscillations in matter and the MSW effect	5
1.3	The Standard Solar Model	6
1.3.1	The nuclear fusion processes	7
1.3.2	The solar neutrino spectrum	9
1.4	Overview on solar neutrino experiments	11
1.4.1	Radiochemical detectors	11
1.4.2	Water Cherenkov detectors	12
1.4.3	Liquid Scintillator detectors	13
2	The BOREXINO experiment	15
2.1	Detector design	15
2.2	The ECHIDNA analysis software	18
2.3	Background supression and data analysis in BOREXINO	20
2.4	Physics program and previous results of BOREXINO	23
3	Spectral Analysis	27
3.1	Simulation of β Spectra	27
3.1.1	Parameterization of allowed β Decays	28
3.1.2	Parameterization of forbidden β Decays	29
3.2	The Fermi Function	30
3.2.1	Parameterization of the Fermi Function	30
3.2.2	Comparison between Approximation and Parameterization of the Fermi function	32
3.3	Simulation of ν Recoil Spectra	33
3.4	Calculation of the Detecor response	34
3.4.1	Quenching Effects	34
3.4.2	Energy Resolution	36

3.5	The χ^2 Fitting Procedure	37
4	Spectral Fits on BOREXINO Monte Carlo Data	39
4.1	Fits on Background Sources	40
4.1.1	^{11}C Spectrum	40
4.1.2	^{85}Kr Spectrum	40
4.1.3	^{210}Bi Spectrum	42
4.2	Fits of Solar Neutrino Spectra	45
4.2.1	^7Be - ν Spectrum	45
4.2.2	The pep- ν Spectrum	45
5	Spectral Fits on Experimental Data of the BOREXINO Experiment	47
5.1	Fit on ^{11}C Spectrum selected by TFC	47
5.2	Combined Spectral Fit of Background and Neutrino Sources	48
5.2.1	Data Selection	49
5.2.2	Spectral Analysis with free contingent of pep ν events	50
5.3	^{40}K as possible Background Source for the pep Neutrinos	54
6	Summary of the results concerning spectral analysis in the BOREXINO experiment	57
7	Neutrino Oscillometry in LENA	61
7.1	The LENA Experiment	61
7.2	Neutrino Oscillometry with ^{51}Cr as monoenergetic neutrino source	64
7.3	Sensitivity of the Spectral Fit on a ^{51}Cr signal with ^7Be Background	66
8	Conclusion and Outlook	69

Chapter 1

Neutrino characteristics and the Standard Solar Model

The discovery of radioactivity more than one century ago opened a new field of research today known as particle physics. Since then, scientists have been extremely successful in broadening the comprehension of elementary particles and their interactions. The knowledge about the Standard Model of particle physics is summarized in the first section of this chapter, providing an overview on the most important characteristics of the particles which are today regarded as structureless at the smallest measurable distances.

However, the neutrino is one particle whose properties are hard to observe, as it only interacts weakly with matter. Therefore 40 years of neutrino experiments still left open questions, particularly on the neutrino mass and mixing angles. The second section illustrates the known characteristics of the neutrino with emphasis on neutrino physics beyond the Standard Model, concerning neutrino oscillations in vacuum and matter as well as the Mikheyev-Smirnov-Wolfenstein (MSW) effect. This effect is important for solar neutrinos which are emitted during the fusion processes in the Sun. The Standard Solar Model which established itself as a good description of these processes will be introduced in the third section, before a short overview on different solar neutrino experiments will be given at the end of this chapter.

1.1 The Standard Model of particle physics

In nature, there are four known kinds of interactions between particles: the gravitational, electromagnetic, weak and strong interaction. As the name indicates, the strong force produces the most powerful interaction and its relative strength is normalized to 1. The relative strength of the electromagnetic force is given by the fine-structure constant $\alpha = \frac{1}{137}$ and in comparison to the strong force, it is three

Quarks	Masses	Charge	Interactions
u c t	1.5 to 3.3 MeV/1.27 GeV/171.2 GeV	$+\frac{2}{3} e$	} strong, electromagnetic and weak
d s b	3.5 to 6.0 MeV/104 MeV/4.2 GeV	$-\frac{1}{3} e$	

Leptons	Masses	Charge	Interactions
e μ τ	511 keV/106 MeV/1.78 GeV	$-1 e$	electromagnetic, weak
ν_e ν_μ ν_τ	0	0	only weak

Gauge Bosons	Masses	Charge	Interaction	Symmetry
γ	0	0	electromagnetic	U(1), QED
W^\pm / Z^0	80.4 GeV / 91.2 GeV	$\pm 1 e / 0$	weak	SU(2), GSW
g	0	0	strong	SU(3), QCD

Table 1.1: Summary of the fundamental characteristics of the elementary particles, the fermions and the gauge bosons, in the Standard Model. Values for the masses are taken from [1].

orders of magnitude weaker. The weak and the gravitational interaction have a relative strength of 10^{-5} and 10^{-38} , respectively. For this reason, the gravitational force is usually neglected in particle physics.

According to the Standard Model of particle physics, all matter is formed out of twelve elementary particles: six quarks and six leptons. Table 1.1 shows their fundamental characteristics. All these particles have a spin of $\frac{1}{2}$ and are therefore fermions.

The masses of the three light quarks (u, d, s) are situated in the MeV range, the heavy quarks (c, b, t) have masses of several GeV. In addition to an electric charge of $+\frac{2}{3} e$ for the so-called up-type quarks and $-\frac{1}{3} e$ for down-type quarks, quarks are the only fermions carrying a colour charge. Thus, quarks can participate in all interactions: electromagnetic, weak and strong. Under the influence of the strong

force, they build colourless (white) bounded states of two and three quarks, which are called mesons and baryons, respectively.

The leptons are separated into charged and neutral particles. The charged leptons (electron, muon and tauon) have masses from MeV up to GeV and carry an electric charge of $-1 e$. The corresponding neutrinos are electrically neutral and regarded as massless in the Standard Model. Therefore, neutrinos only interact via the weak force, whereas the charged leptons participate in the electromagnetic interaction, too.

The interactions in the Standard Model are described by different gauge symmetries (see Table 1.1). The number of generators of the corresponding groups is equal to the number of gauge bosons: One photon for the electromagnetic, two charged and one neutral bosons for the weak and eight gluons for the strong interaction, as the group $SU(n)$ has $n^2 - 1$ generators. The three gauge bosons of the weak interaction are the only massive ones. The mass of the gauge bosons influences the range of the interaction. The electromagnetic interaction with the massless photon as gauge quantum has infinite range. On the contrary, the weak interaction has a quite short range (less than the radius of an atomic nucleus) due to the massive W^\pm and Z^0 bosons, as the propagator is antiproportional to the squared boson masses.

Following this argument, the strong interaction should have infinite range, too, as gluons are massless. However, gluons carry a colour quantum number which can cause self-interactions and decreases the range to a distance of about 1 fm.

Besides the presented fundamental fermions, the Standard Model includes the same number of antifermions. The antiparticles have the same mass as the particles, but the opposite electric charge.

1.2 Characteristics of neutrinos

In 1930, Wolfgang Pauli proposed a new particle, the neutrino, to explain the conservation of energy and angular momentum in β decays [2]. In the Standard Model of Particle Physics, these neutrinos, described as the electrically neutral partner of the corresponding lepton, are massless and only weakly interacting particles. Furthermore, they have a fixed helicity (left-handed neutrinos, right-handed antineutrinos) and violate parity maximally.

The exchange of W^\pm and Z^0 bosons defines a charged current (CC) and a neutral current (NC) interaction. While the NC is always flavor conserving, the CC converts neutrinos in the charged lepton of the same family and vice versa. CC interactions do not obligatorily conserve the flavor.

However, after more than 40 years of neutrino experiments, there are still a lot of open questions concerning the characteristics of neutrinos, as e.g. if it is a Dirac or

Majorana particle, or the possible existence of heavy right-handed (seesaw-model) or sterile neutrinos and the stability of these particles.

Since the first neutrino experiments (see section 1.4), it has become obvious that physics beyond the Standard Model is necessary to describe the results of neutrino properties. For instance, the deviation between the predicted neutrino rate from solar models and the measured rate in neutrino experiments is explained by neutrino oscillations, which require massive neutrinos. Today the known upper limit for the mass of the lightest neutrino from experimental data is $m_i < 2.0 \text{ eV}$ [1].

1.2.1 Neutrino oscillations in vacuum

The neutrino flavor eigenstates $|\nu_\alpha\rangle$ ($\alpha = e, \mu, \tau$) participating in the weak interaction do not necessarily coincide with the neutrino mass eigenstates $|\nu_i\rangle$ ($i = 1, 2, 3$). The transition between these two bases is described by an unitary 3×3 matrix, comparable to the CKM¹ mixing matrix in the quark sector. Therefore, $|\nu_\alpha\rangle$ can be expressed in terms of the mass eigenstates $|\nu_i\rangle$ and vice versa:

$$\begin{pmatrix} \nu_e \\ \nu_\mu \\ \nu_\tau \end{pmatrix} = U \begin{pmatrix} \nu_1 \\ \nu_2 \\ \nu_3 \end{pmatrix} \quad \Rightarrow \quad |\nu_\alpha\rangle = \sum_i U_{\alpha i} |\nu_i\rangle \quad |\nu_i\rangle = \sum_\alpha U_{i\alpha}^\dagger |\nu_\alpha\rangle \quad (1.1)$$

The unitary matrix U in equation 1.1, called the Pontecorvo-Maki-Nakagawa-Sakata (PMNS) matrix [3], can be parameterised by three mixing angles θ_{ij} and one CP-violating phase δ ($c_{ij} = \cos\theta_{ij}$, $s_{ij} = \sin\theta_{ij}$):

$$U = \begin{pmatrix} 1 & 0 & 0 \\ 0 & c_{23} & s_{23} \\ 0 & -s_{23} & c_{23} \end{pmatrix} \begin{pmatrix} c_{13} & 0 & s_{13}e^{-i\delta} \\ 0 & 1 & 0 \\ -s_{13}e^{-i\delta} & 0 & c_{13} \end{pmatrix} \begin{pmatrix} c_{12} & s_{12} & 0 \\ -s_{12} & c_{12} & 0 \\ 0 & 0 & 1 \end{pmatrix} \quad (1.2)$$

As solutions of the Schrödinger equation, the mass eigenstates propagate in time as

$$|\nu_i(t)\rangle = e^{-iE_i t} |\nu_i(0)\rangle \quad (1.3)$$

Under the assumptions that the neutrinos are highly relativistic and every mass eigenstate of the neutrino has the same momentum p , the energy E_i of the mass eigenstate can be approximated to

$$E_i = \sqrt{p^2 + m_i^2} \approx E + \frac{m_i^2}{2E} \quad (1.4)$$

with the neutrino energy E .

As all $|\nu_i\rangle$ have different masses, the eigenstates $|\nu_i(t)\rangle$ propagate with different

¹Cabibbo Kobayashi Maskawa

Parameter	$\sin^2(2\theta_{12})$	$\sin^2(2\theta_{23})$	$\sin^2(2\theta_{13})$	δm_{21}^2 in 10^{-5}eV^2	$ \delta m_{32}^2 $ in 10^{-3}eV^2
Value	0.87 ± 0.03	> 0.92	< 0.15	7.59 ± 0.20	2.43 ± 0.13

Table 1.2: The best values and limits for the oscillation parameters in vacuum. The sign of δm_{32}^2 has to be positive due to the MSW effect, whereas the sign of δm_{32}^2 is not known, yet (values taken from [1]).

velocities and as a flavor eigenstate $|\nu_\alpha\rangle$ is a superposition of all three mass eigenstates, a neutrino of flavor α can be detected as a neutrino of a different flavor β after travelling the distance x . The probability for such a transition is

$$\begin{aligned}
 P_{\alpha\rightarrow\beta} &= |\langle\nu_\beta|\nu_\alpha(t)\rangle|^2 = |\langle\nu_\beta|U|\nu_i(t)\rangle|^2 = |\langle\nu_\beta|Ue^{-iE_it}|\nu_i\rangle|^2 = |\langle\nu_\beta|Ue^{-iE_it}U^\dagger|\nu_\alpha\rangle|^2 \\
 &\simeq \sum_{ij} U_{\alpha i}U_{\alpha j}^*U_{\beta i}^*U_{\beta j} e^{-i(\frac{\delta m_{ij}^2}{2E})t} \quad (1.5)
 \end{aligned}$$

In this notation δm_{ij}^2 stands for the difference of the squared neutrino masses $\delta m_{ij}^2 = m_i^2 - m_j^2$ and $|\nu_\alpha(t)\rangle$ describes the development of the flavor eigenstate α in time. Table 1.2 gives the current limits for the three mixing angles and mass differences.

In the case of solar neutrinos, oscillations via the mixing angle θ_{13} can be neglected as $\sin^2(2\theta_{13}) \ll 1$ and the oscillation can be described by two-flavor approximation with

$$U = \begin{pmatrix} \cos\theta_{12} & \sin\theta_{12} \\ -\sin\theta_{12} & \cos\theta_{12} \end{pmatrix} \quad (1.6)$$

In this simplification, the probability for a solar neutrino produced in the eigenstate $|\nu_e\rangle$ to be detected in the same eigenstate after travelling the distance L to the earth is calculated to

$$P_{\nu_e\rightarrow\nu_e} = 1 - \sin^2(2\theta_{12}) \cdot \sin^2\left(\frac{\delta m_{21}^2}{4E}L\right) \quad (1.7)$$

It becomes clear from equation 1.7 that the oscillations would vanish if the neutrinos were massless: The mass difference δm_{21}^2 gives the frequency whereas the mixing angle θ_{12} determines the amplitude of the oscillations.

Averaging over long distances (high number of oscillations), the survival probability depends only on the mixing angle and equation 1.7 simplifies to

$$\langle P_{\nu_e\rightarrow\nu_e} \rangle = 1 - \frac{1}{2}\sin^2(2\theta_{12}) \quad (1.8)$$

1.2.2 Neutrino oscillations in matter and the MSW effect

Neutrino oscillations in matter are different from the oscillations in vacuum due to the interactions of the neutrinos with the electrons of the material they are travelling through. While all flavor eigenstates interact with normal matter only by

NC interactions, $|\nu_e\rangle$ alone can also interact via CC with electrons. When calculating the oscillation probability in matter, this fact is described by an additional potential V operating on $|\nu_e\rangle$ that is equivalent to an effective mass term for the electron neutrino [3, 4, 5]:

$$V = \sqrt{2}G_F N_e \quad (1.9)$$

$$m_{em}^2 = m_{ee}^2 + A \approx m_{ee}^2 + 2\sqrt{2}G_F N_e E \quad (1.10)$$

with G_F the Fermi coupling constant, N_e the number of electrons in the matter and E the neutrino energy.

This corresponds to an additional rotation for the mass eigenstates for neutrinos in matter with respect to the mass eigenstates in vacuum. The resulting mass difference and the mixing angle in matter for the two flavor approximation are

$$\Delta m_{12,m}^2 = \delta m_{12}^2 \sqrt{\left(\frac{A}{\delta m_{12}^2} - \cos(2\theta_{12})\right)^2 + \sin^2(2\theta_{12})} \quad (1.11)$$

$$\sin^2(2\theta_m) = \frac{\sin^2(2\theta_{12})}{\left(\frac{A}{\delta m_{12}^2} - \cos(2\theta_{12})\right)^2 + \sin^2(2\theta_{12})} \quad (1.12)$$

As a consequence, the survival probability 1.8 in matter is depending on the neutrino energy E and the density of the electrons in the considered matter.

Equation 1.12 describes a resonance curve which leads to a maximum in the oscillation amplitude and therefore to a complete conversion of $|\nu_e\rangle$ to $|\nu_\mu\rangle$ for $A = \delta m_{12}^2 \cdot \cos(2\theta_{12})$. For the electron neutrinos produced by the fusion processes within the Sun, this resonance becomes important. Travelling from the interior to the surface of the Sun, the electron neutrino experience a change in the matter density. As the energy spectrum of the solar neutrinos (see figure 1.3) cover a broad range from a few keV up to several MeV, this resonant flavor changing can be observed on solar neutrinos with energies higher than ~ 1 MeV and is especially affecting the measured rate of solar ^8B , hep and pep neutrinos.

This explanation for the deviation between the predicted solar neutrino rates and the measured rates in the solar neutrino experiments was first proposed by Mikheyev, Smirnov and Wolfenstein and is therefore called the MSW effect [4, 6].

1.3 The Standard Solar Model

The Sun is characterised as a main sequence star, burning hydrogen to helium during nuclear fusion processes. In contrast to photons, the neutrinos provide a direct look into the solar center as they are only weakly interacting and do not participate in electromagnetic scattering processes in solar matter. Therefore, they

are important messengers for the observation of the Sun.

In the Standard Solar Model, the equations of states describing the evolution of the Sun are derived by the following basic assumptions [7,8]:

- **Hydrostatic equilibrium:**

The gravitational attraction is equal to the thermal pressure of the solar matter. A violation of this equilibrium would lead to a collapse or expansion of the Sun.

- **Thermal equilibrium:**

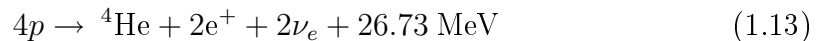
The energy produced within the Sun has to be equal to the emitted energy on the surface. Small deviations of this equilibrium can be balanced by an adjustment of the gravitational energy.

- **Energy generation and transport:**

The energy is generated by nuclear fusion processes close to the solar center. The transport in the interior of the Sun is dominated by photon diffusion processes with an additional contribution of convective motions near the solar surface.

1.3.1 The nuclear fusion processes

The nuclear fusion processes take place in the core of the Sun where hydrogen is burned to helium. This can be summarized by the effective fusion reaction:



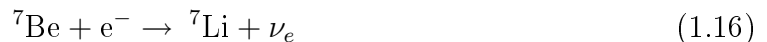
which is valid for both of the reaction chains: The pp chain and the CNO cycle.

The pp fusion chain

Figure 1.1 shows all fusion reactions of the pp chain with their branching ratios. The reaction chain can be started either by the pp or pep reaction:



The further devolution is divided into four chains, all terminating with the production of ${}^4\text{He}$. The nuclear reactions emitting neutrinos during this process are:



The electron capture (EC) decay of ${}^7\text{Be}$ produces two neutrino lines due to an excited state of ${}^7\text{Li}$ with a ratio of 90% and 10%, respectively (see table 1.3).

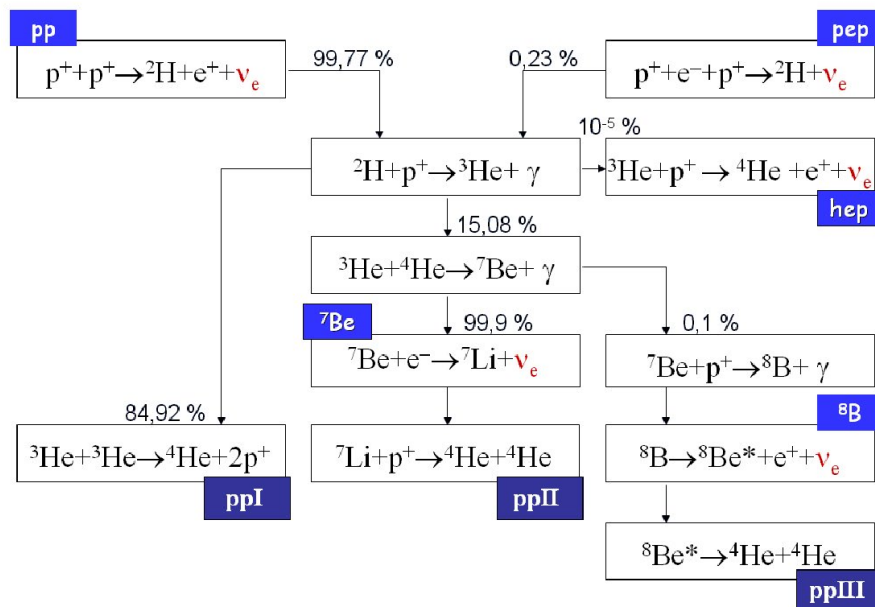


Figure 1.1: Schematic view of the pp fusion cycle. The number next to the arrow denote the branching ratio of the corresponding fusion process [9].

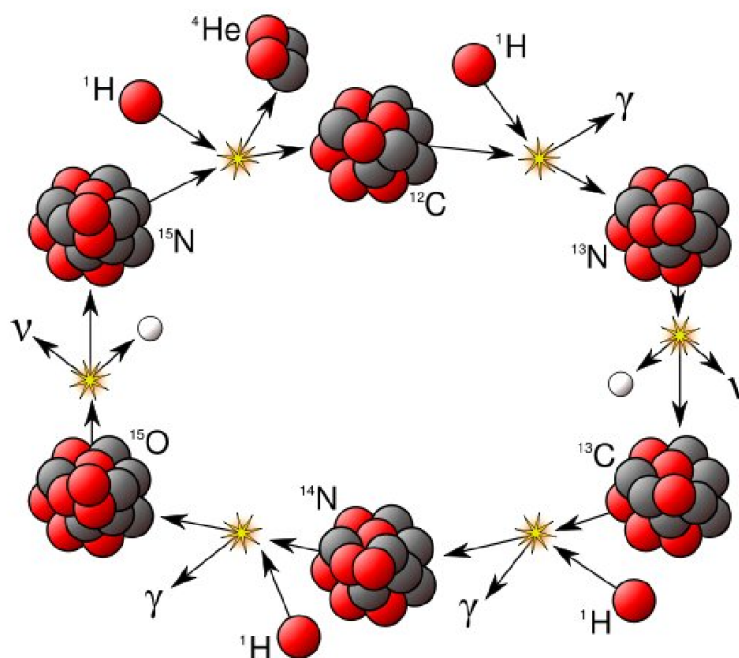


Figure 1.2: Schematic view of the CNO-I fusion cycle [9].

Source	Flux in cm^2s^{-1}	E_{ν_e} in MeV
pp	$5.99 \cdot 10^{10}$	≤ 0.420
pep	$1.42 \cdot 10^8$	$= 1.442$
hep	$7.93 \cdot 10^3$	≤ 18.773
${}^7\text{Be}$	$4.84 \cdot 10^9$	$= 0.862$ (89.7%) $= 0.384$ (10.3%)
${}^8\text{B}$	$5.69 \cdot 10^6$	< 15.0
${}^{13}\text{N}$	$3.05 \cdot 10^8$	≤ 1.199
${}^{15}\text{O}$	$2.31 \cdot 10^8$	≤ 1.732
${}^{17}\text{F}$	$5.83 \cdot 10^6$	≤ 1.740

Table 1.3: Solar neutrino fluxes at Earth [10] and neutrino energies [11] of the nuclear fusion processes.

The CNO fusion cycle

The CNO-I cycle shown in figure 1.2 is a catalytic process on ${}^{12}\text{C}$. As the Coulomb barriers for these reactions are higher than for the pp chain and the mass of the Sun is too low to provide high enough temperatures, the CNO cycle is subdominant and participates only with $\approx 2\%$ to the total energy production.

The reactions emitting neutrinos are the β^+ decays of nitrogen, oxygen and fluorine:



1.3.2 The solar neutrino spectrum

As mentioned before, solar neutrinos provide an undisturbed look on processes inside the Sun due to their weak interaction. Furthermore, the Sun is a steady source of neutrinos, produced during nuclear fusion process, and offers therefore a good possibility of studying these particle. For this reasons, the solar neutrino flux on Earth is of interest for particle physics as well as for astrophysics.

The total neutrino flux emitted by the Sun can be estimated by using the solar luminosity $L_\odot \simeq 3.84 \cdot 10^{26}$ W. As 98% of the energy of the Sun is transported by photons and the production of ${}^4\text{He}$ emits two neutrinos, the calculation using the luminosity constraint [14] gives a total neutrino flux of

$$\Phi_{\nu_e} \simeq 2 \cdot \frac{1}{4\pi d^2} \cdot \frac{L_\odot}{Q} \simeq 6.4 \cdot 10^{10} \text{ cm}^{-2}\text{s}^{-1} \quad (1.22)$$

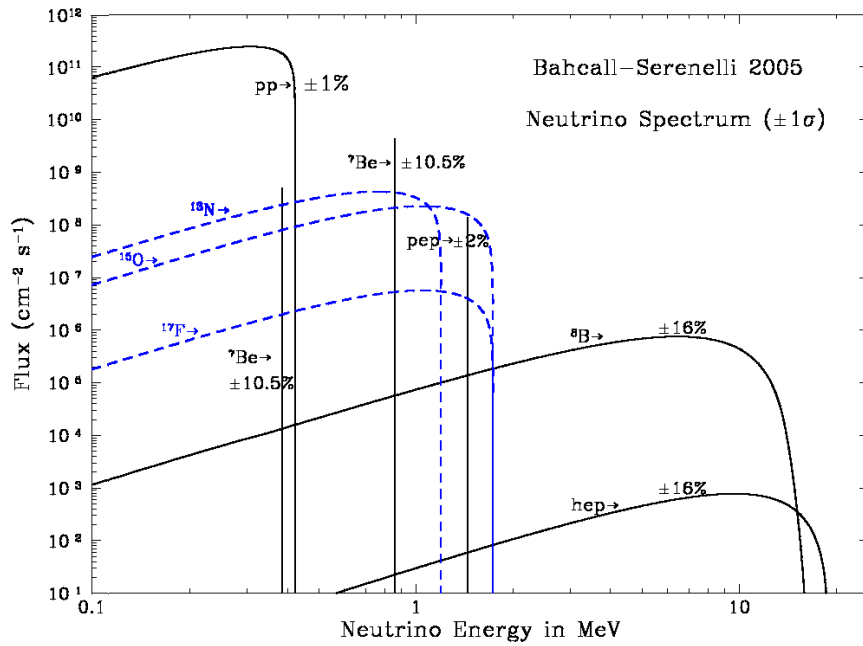


Figure 1.3: The solar neutrino energy spectrum calculated for the solar model BS05(OP) [12].

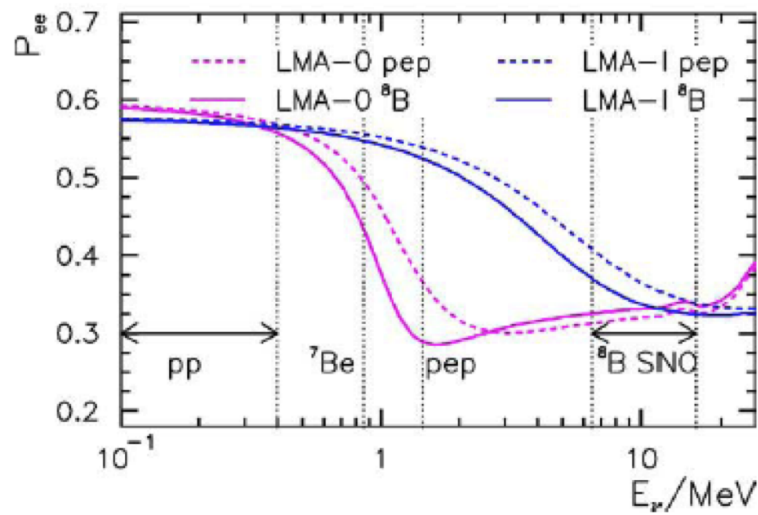


Figure 1.4: The predicted distribution of the survival probability for solar neutrinos due to the MSW effect. The blue line corresponds to a standard LMA solution, the violet line includes nonstandard neutrino interactions [13].

where $d \simeq 1.5 \cdot 10^8 \text{km}$ is the averaged distance between the Earth and the Sun and Q is the released energy during the ${}^4\text{He}$ fusion (see equation 1.13).

Table 1.3 summarizes the fluxes and energy range of the different neutrino sources, whereas figure 1.3 shows the energy spectrum of the solar neutrinos as derived from Standard Solar Model calculations.

As stated in section 1.2.2 the neutrinos have to travel through the inhomogeneous density of the solar matter and partly undergo the MSW effect. Figure 1.4 illustrates the survival probability for electron neutrinos. The energy range below $\approx 1 \text{ MeV}$ is dominated by vacuum oscillations, for energies higher than $\approx 4 \text{ MeV}$ the survival probability is reduced dramatically due to matter oscillations. Both energy regions are by now measured via the observation of the ${}^7\text{Be}$ (see section 2.4) and ${}^8\text{B}$ (see section 1.4.2 and 2.4) solar neutrinos and the survival probabilities are well determined.

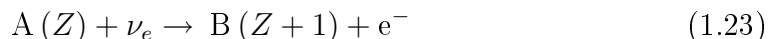
However, the energy range from 1 MeV to 4 MeV is particularly interesting as the transition region between vacuum and matter oscillations possibly shows deviations from the standard MSW LMA solution due to nonstandard interactions, e.g. by introduction of sterile neutrinos (see figure 1.4). Depending on the model, these deviations can be quite strong, which might provide the possibility to distinguish them from the standard MSW LMA model. Considering their energy of 1.442 MeV, the solar pep neutrinos are the most promising candidates to test the transition region and put further constraints on the survival probability. Therefore, the search for this neutrinos and the determination of the pep neutrino flux are important issues for solar neutrino experiments today.

1.4 Overview on solar neutrino experiments

This section will give an overview on the detection techniques used in solar neutrino experiments. From the first experiment in 1970 up to now all detectors can be classified to one of the three groups: Radiochemical, water Cherenkov or liquid scintillator detector.

1.4.1 Radiochemical detectors

Radiochemical detectors measure solar neutrinos via the capture of the neutrino at a target atom (CC interaction):



For this kind of experiment, the choice of the target nucleus with regard to a low energy threshold for reaction 1.23 is crucial. Furthermore, the half-live of the daughter nucleus should be in the order of a few weeks to ensure an appropriate

exposure time. Afterwards, the molecules of the neutrino induced isotope have to be chemically separated from the target atoms. The detection of the solar neutrinos is done by the observation of the decay of the daughter nucleus. Radiochemical experiments are sensitive to the time and energy integrated neutrino flux and therefore provide directional and only limited spectral info.

The Homestake experiment [15] operated by R. Davis and his collaborators was the first solar neutrino experiment. The detector was based on a 615 t target of tetrachloroethylene (C_2Cl_4) and located at the Homestake gold mine providing a shielding of (4200 m.w.e.). The reaction



has an energy threshold of 814 keV and thus is only sensitive to solar ^8B and CNO neutrinos. The ^{37}Ar atoms were separated by flushing the target volume with helium and their decay was detected in miniature proportional counters. Starting in 1970 the experiment took almost 30 years of data, measuring the solar neutrino flux to

$$\Phi_{\nu_e} = 2.56 \pm 0.16_{\text{stat}} \pm 0.16_{\text{sys}} \text{ SNU}^2 \quad (1.25)$$

This result has to be compared with the predictions of standard solar models which vary from 6.4 SNU to 9.3 SNU. Therefore, the detected neutrino rate is far to low. Other radiochemical experiments such as GNO, GALLEX [16] and SAGE [17] (all based on ^{71}Ga as target material) confirmed these observation. This caused the so-called Solar Neutrino Problem which was finally solved by the discovery of neutrino oscillations.

For his great achievements in the field of neutrino astronomy, R. Davis was awarded the Nobel Price in Physics in 2002.

1.4.2 Water Cherenkov detectors

If a charged particle travels through matter at a velocity higher than the speed of light in this matter, it emits Cerenkov light in a cone along its course. Detected by optical sensors, such as photomultiplier tubes (PMTs), this light provides the possibility of reconstructing track and position of the observed particle in real-time. As neutrinos are neutral particles, they do not produce Cerenkov light by themselves. Instead, they transfer part of their energy to the electrons in the water by elastic scattering:



Thus the neutrino is detected indirectly via the Cherenkov light of the electron. However, current water Cherenkov detectors have a high energy threshold (\approx

²1 SNU = 10^{-36} events /s /target atom

4 MeV) due to intrinsic background signals and a low light yield. Therefore, this detection technique is only sensitive to the high-energetic ^8B neutrinos.

Two prominent examples for water Cherenkov detectors are the Kamiokande detector [18] and its successor Super-Kamiokande [19]. The Super-Kamiokande experiment consists of a cylindrical detector filled with 50 kton of ultra pure water which is located at the Kamioka Observatory in Japan (≈ 2700 m.w.e.). It is separated into an Inner Detector (ID) and an Outer Detector (OD), so that the OD can be used as muon veto.

The measurements during the third phase of the Super-Kamiokande detector (SK-III) from October 2006 to August 2008 gave a ^8B solar neutrino flux of [20]

$$\Phi_{s_B} = 2.32 \pm 0.04_{\text{stat}} \pm 0.05_{\text{sys}} \cdot 10^6 \text{ cm}^2\text{s}^{-1} \quad (1.27)$$

This result is in agreement with the radiochemical experiments, the Kamiokande experiment and the former Super-Kamiokande measurements SK-I and SK-II.

The SNO (Sudbury Neutrino Observatory) detector is located in the Vale Inco's Creighton Mine in Canada (5890 m.w.e.) [21]. In contrast to the other described experiments its spherical volume is filled with 1000 t of heavy water (D_2O) and shielded by more than 7 ktons of light water.

Due to the deuterium, neutrinos can be detected by three different processes:

$$\nu_x + e^- \rightarrow \nu_x + e^- \quad (\text{ES})$$

$$\nu_e + d \rightarrow p + p + e^- \quad (\text{CC})$$

$$\nu_x + d \rightarrow p + n + \nu_x \quad (\text{NC})$$

This allowed for the first time to distinguish between signals from electron neutrinos by the CC reaction and the comined signals of all flavors via the NC channel. While the measured flux in the ES and the CC channel is consistent with the results of earlier experiments, has the total flux of the ^8B solar neutrinos been determined to

$$\Phi_{s_B} = 5.046 \begin{matrix} +0.159 \\ -0.152 \end{matrix} (\text{stat}) \begin{matrix} +0.107 \\ -0.123 \end{matrix} (\text{sys}) \cdot 10^6 \text{ cm}^2\text{s}^{-1} \quad (1.28)$$

which is consistent with the prediction of the Standard Solar Model. The result confirmed neutrino oscillations to be the solution to the Solar Neutrino Problem.

1.4.3 Liquid Scintillator detectors

Detectors with a target of liquid scintillator also observe neutrinos via neutrino-electron scattering. The energy of the recoil electron is deposited in the detector

by exciting scintillator molecules, which emit this energy isotropically as UV-light. Liquid scintillator detectors provide a higher light yield than water Cherenkov detectors and a lower energy threshold (a few 100 keV), limited by radioactive background. Therefore, these detectors are the first ones which can measure solar neutrinos in the sub-MeV range in real time.

Two experiments based on this detection technique are KamLAND (Kamioka Liquid scintillator Anti-Neutrino Detector) [22] and BOREXINO (see chapter 2). Both detectors have a similar setup: A spherical inner detector containing the target is surrounded by a buffer liquid for shielding and a water Cherenkov detector used as active muon veto.

KamLAND is located the former site of the Kamiokande experiment and was originally build to detect reactor antineutrinos. However, after starting a purification campaign in 2007, the experiment will be changed to a solar neutrino experiment.

Chapter 2

The BOREXINO experiment

Proposed in the late 80's, the BOREXINO detector was the first experiment with an energy threshold low enough to detect sub-MeV solar neutrinos in real-time. This ambitious goal set strong demands at the level of radiopurity and the features of the chosen scintillator, as the expected rate of the solar neutrinos are only a few tens of events per day. A small prototype of BOREXINO, the Counting Test Facility (CTF), was built at the beginning of the 90's with a target mass of 4 t. Even though being much smaller, it had many characteristics of the originally experiment and proved with great success the feasibility of BOREXINO.

With this encouraging result, the collaboration built the BOREXINO detector between 1996 and 2004 in Hall C of the Laboratori Nazionali del Gran Sasso (LNGS) in Italy. The filling of the detector with liquid scintillator finished in 2006 and after testing the system, data is taken since 16th May 2007.

This chapter starts with a description of the main parts and characteristics of the BOREXINO detector [23, 24]. Furthermore the software tools for the data reconstruction and analysis will be introduced. The third section is dedicated to the background sources and their rejection by coincidence analysis and the end of this chapter will give an overview on the first results achieved by BOREXINO so far.

2.1 Detector design

The BOREXINO experiment is based on a liquid scintillator detector, observing solar neutrinos via neutrino-electron scattering. The scattered electron deposits its energy in the scintillator producing a light signal that is detected by photomultiplier tubes (PMTs).

The design of the BOREXINO detector is shown in figure 2.1. It is divided into an Inner Detector (ID) and an Outer detector (OD). Starting at the center, the ID includes the spherical Inner Vessel (IV), the Outer Vessel (OV) and the Stainless Steel Sphere (SSS), whereas the OD is a water Cherenkov detector. With this

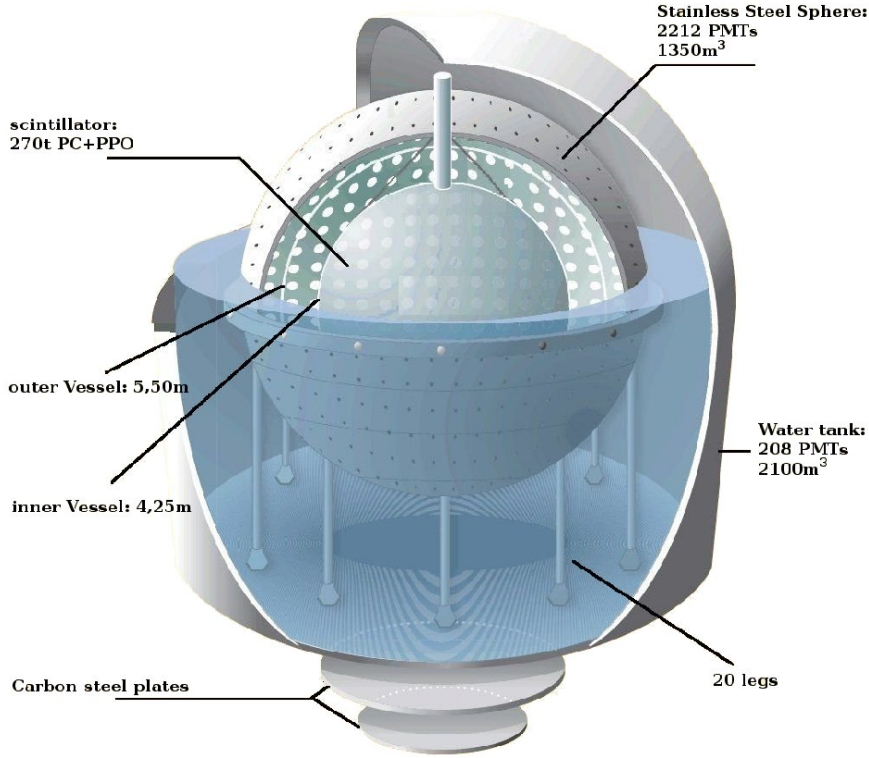


Figure 2.1: Design of the BOREXINO detector. The target volume located in the center of the detector is surrounded by the buffer liquid and the water tank to shield it from external neutron and γ background [25].

setup of the detector, the target volume inside the IV is shielded by a buffer liquid and the ultra pure water of the OD, resulting in an increasing radiopurity from the outside to the inside of the experiment.

All the components and their functions will be described in detail in the following. The electronics and the data acquisition (DAQ) system of the detector are not covered in this work as it would exceed the limit of this thesis. Detailed information on this topics can be found in [24,8].

The Inner Vessel (IV) and the liquid scintillator

The IV is a $125 \mu\text{m}$ thick nylon membrane with 4.25 m radius, which is filled with 270 t of liquid scintillator. After careful studies within the CTF, pseudocumene (PC, 1,2,4-trimethylbenzene, $\text{C}_6\text{H}_3(\text{CH}_3)_3$) was chosen as scintillator solvent with an admixture of $1.5 \frac{\text{g}}{\text{l}}$ (flour) PPO (2,5-diphenyloxazole, $\text{C}_{15}\text{H}_{11}\text{NO}$) as wavelength shifter [26]. The BOREXINO scintillator mixture has a main decay time of 1.3 ns.

The light is emitted at a wavelength of ~ 400 nm and an attenuation length of ~ 7 m. Self-absorption is avoided by shifting the wavelength of this light.

In order to achieve a low energy threshold, a very high level of radiopurity is needed. Therefore, the PPO and the nylon used for the IV were purified carefully when building the detector. The impurity of the primordial isotopes ^{238}U and ^{232}Th could be reduced to $(1.6 \pm 0.1) \cdot 10^{-17}$ g and $(6.8 \pm 1.5) \cdot 10^{-18}$ g per gram of scintillator, respectively [27]. However, due to a contribution of natural ^{14}C present in the liquid scintillator, the effective energy threshold is about 200 keV.

The Outer Vessel (OV) and the buffer liquid

In order to shield the IV from external γ background, the region between the IV and the SSS is filled with 1040 t of a buffer liquid which is composed of PC and $5 \frac{\text{g}}{\text{l}}$ dimethylphthalate (DMP). The DMP is necessary to reduce the scintillation light produced by the PC molecules. The light signal of the buffer liquid is quenched by a factor ~ 20 ensuring that the dominant signal comes from the target material inside the IV. With PC as the main element of the buffer liquid, the hydrostatic pressure applied to the IV is reduced to a minimum..

The OV is a second nylon membrane with 5.50 m radius working as a diffusion barrier to the noble gas ^{222}Rn which is emitted by construction material (e.g. steel or the glass of the photomultiplier tubes).

The Stainless Steel Sphere (SSS) and the photomultiplier tubes (PMTs)

The SSS is the central support structure of the detector and has a radius of 6.85 m. All PMTs (8", ETL 9351) of the ID are attached to the SSS. In total there are 2212 PMTs observing the ID, 1838 of them being equipped with optical concentrators (Winston cones) resulting in a total optical coverage of $\sim 30\%$. With the nylon vessels, the liquid scintillator and the buffer liquid having almost the same refractive index, these detector components do not influence the photon propagation leading to a proper spatial resolution [24].

The Outer Detector (OD): A water Cherenkov detector

The OD consists of a 17 m high steel dome with 9 m radius. It is filled with 2100 t of ultra pure, deionized water. 208 PMTs mounted on the SSS and on the bottom of the water tank collect the Cherenkov light produced by charged particles.

As the BOREXINO detector is located in the LNGS, which provides a rock shielding of ~ 3800 m.w.e., the flux of cosmic muons is reduced by six orders of magnitude. However, there is still a flux of about $1 \text{ muon m}^{-2}\text{h}^{-1}$ producing cosmogenic background inside the IV. Therefore, the OD is an essential instrument providing an active muon veto.

2.2 The ECHIDNA analysis software

There are two equivalent codes for offline data reconstruction and analysis within the BOREXINO collaboration: MACH4, the american code, and ECHIDNA which is used by the european members of the collaboration.

The ECHIDNA framework is based on the programming language C++. All source code used for data reconstruction or analysis is compiled with ROOT, a C++ interpreter developed by CERN [28].

All analyses concerning BOREXINO data were performed within the framework of the ECHIDNA software. Therefore, this section will give a short introduction to the main features of data reconstruction in this code and the ECHIDNA software parameters which are important for this thesis. A detailed description of the different ECHIDNA modules can be found in [8].

A typical Data Acquisition (DAQ) run of the BOREXINO detector has a duration of 6 hours. Every time the ID or the OD triggers, a full read out of the detector is performed and the data is saved in a binary file. At the end of the run this rawdata contains the encoded information on the type and time of the trigger as well as the charge and time information of all PMT hits in the ID and OD.

However, in this form the data is not usable for physics analysis. Therefore in a first step the rawdata is decoded by running an electronics calibration on it. The calibration is based on events from laser, LED and pulser hits injected into the detector at the beginning of a run as well as during the run with a frequency of 0.1 Hz. In addition a pure calibration run is taken every week and after every configuration in the detector hardware or electronics.

After decoding the rawdata, a clustering algorithm is performed which identifies real events by searching for time-correlations (clusters) in the decoded hits of the PMTs, calculating their properties and saving them into variables. These variables are organized in a ROOT file in form of a tree structure. All variables containing trigger information are labelled "trigger", the informations concerning the ID are recorded in variables called "laben" (the Laben S.p.A. company produced the electronics of the ID) and the name "muon" refers to the OD. Altogether this procedure provides the advantage that the physics analysis can be performed by macros containing C++ commands reading out the different variables.

The variables which were used for the data analysis performed in this thesis will now be described in more detail:

- *run* and *evnum*: The run number and the eventnumber provide a unique identification of any event.
- *trigger.trgtype*: The triggertype is 1 if the ID triggered and 2 if the only

OD triggered. If the event was identified as a muon-induced neutron, the `triggertype` is equal to 128.

- *trigger.btb_inputs*: The `btb` is an additional trigger information. It is 4 if the ID and the OD triggered which helps identifying muons crossing the detector.
- *trigger.gpstimes*: The GPS time is recorded for every event in seconds or nanoseconds. This plays a role for time correlations between events.
- *laben.n_live_pmts*: This variable gives the number of working logical channels. It can vary between runs due to electrical problems or malfunction of PMTs.
- *laben.n_decoded_hits*: The total number of hits is calculated for every event by adding up the hits of all PMTs for the event.
- *laben.n_clusters*: The number of clusters identified within one event (usually it is 1). However, due to pile-up effects or fast coincidences one event can contain even two or three clusters.
- *laben.clusters.charge*: The sum of the deposited charged within one cluster is given in terms of photoelectrons, referring to the energy of the event.
- *laben.clusters.nhits*: The number of hit PMTs within one cluster.
- *laben.clusters.mean_time* and *laben.clusters.peak_times*: The meantime and peaktime of the hits within one cluster is given relative to the start time of the cluster.
- *laben.position_mi*: The Milan position reconstruction code provides the event position along the x-, y- and z-axis as well as the distance from the center of the detector.
- *tags.phystag*: During offline data reconstruction muon events, fast cosmogenic background and fast coincidences can be identified and tagged. The nature of the event defines the number of the *phystag*.

2.3 Background suppression and data analysis in BOREXINO

Despite the small amount of radioactive background sources in the material of the detector and in the liquid scintillator, it is important to study these background events and to develop techniques for rejecting them in the data. In this context, the number of design for background suppression is as manifold as the background sources.

Intrinsic background

The intrinsic background in BOREXINO originates from small contamination of the liquid scintillator, e.g. due to airleaks generated during refilling operations. These impurities consist of radioactive decays, mostly from the natural U/Th chain, emitting α , β and sometimes γ particles.

The method mainly used to distinguish between α and β decays is the pulse shape discrimination (PSD) [29]. The different pulse shapes of α and β events are caused by the different ionization densities of these particles. Thus, it is possible to identify these particles via the ratio between the entire pulse duration and the tail of the pulse, which provides a tool for statistical subtraction of α decays. As the recoil electron produced by neutrino-electron scattering is not discriminable from β decay events, the PSD is no method to reject this background with regard to the neutrino signal.

However, another possibility to tag intrinsic background is the search for fast coincidences between mother and daughter nuclide, which is feasible for short half lifes of the daughter isotope. In the BOREXINO data this signal is identified via coincidences in spatial, time and energy between two independent events. A good example is the decay of ^{214}Bi into ^{214}Po ($T_{\frac{1}{2}} = 164\mu\text{s}$). If this background is present within the data, there have to be two events with the following characteristics:

- The first event fits the energy range of the ^{214}Bi β decay.
- The second event has to fit the energy of the ^{214}Po α decay and simultaneously to be within a time window of a few times the half life of ^{214}Po with regard to the first event.
- Under the assumption that the mother and the daughter nuclide are at rest, the second event has to occur at the same position within the detector as the first event.

Events fulfilling these conditions are tagged as background and can be removed from the data.

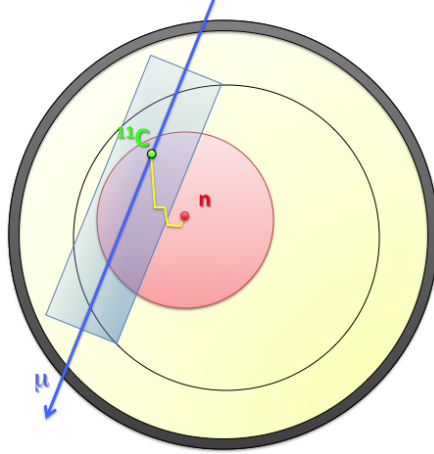


Figure 2.2: Schematic visualisation of the Three-fold Coincidence technique. The cosmogenic radionuclide ^{11}C is tagged by the identification of a muon crossing the IV in coincidence with a neutron and the β decay of the ^{11}C isotope itself (picture taken from [27]).

Cosmogenic background

At the LNGS the flux of cosmic muons is reduced by about six orders of magnitude, compared to surface level. The remaining muon flux is $\sim 1 \text{ m}^{-2}\text{h}^{-1}$. These high-energetic muons produce so-called cosmogenic background inside the target volume via nuclear reactions with the carbon atoms of the liquid scintillator.

Whereas short-lived cosmogenic radionuclides ($T_{\frac{1}{2}} \ll 1 \text{ s}$) can be avoided by applying a time cut after a muon event, an efficient tagging procedure is needed to identify long-lived radionuclides within the data. The Three-fold Coincidence technique (TFC), illustrated in figure 2.2, provides such a tool especially for the radionuclides ^{11}C and ^{10}C [30].

The main idea of the TFC is, that a muon producing other carbon isotopes out of ^{12}C has to knock off at least one neutron, which will be captured by a proton and therefore can be identified by the emitted 2.2 MeV γ :



As the range of the neutron in the liquid scintillator is very limited, the decay of the carbon isotope has to be seen within a defined radius and time window (determined by the half live of the nuclide) with regard to the neutron event.

External background

All material installed inside the detector (e.g. the nylon vessels, the stainless steel sphere, the glass of the PMTs) contain natural radioactive sources. As this radiation enters the target volume from the outside, it is referred to as external background.

Usually, α and β particles are shielded from the liquid scintillator by the buffer liquid. However, high-energetic γ quanta and all radiation which is emitted on the surface of the IV can easily produce a signal in the outer part of the target volume. As the signal of this background is decreasing exponentially from the outside to the center of the IV, a reduced fiducial volume (FV) of the IV is defined. In BOREXINO the typical FV has a radius of $r = 3.021$ m which corresponds to a mass of 100 t. With this restriction a great part of the external background can be rejected without losing much statistics.

Data analysis

In principle, there are two possible techniques of analysing data: Coincidence analysis (e.g. TFC) and spectral fits (see chapter 3).

Figure 2.3 shows a typical energy spectrum as it is obtained by the BOREXINO detector after 300 days of measurement. A muon cut, a fast coincidence cut and a FV cut have been applied. As result, the ${}^7\text{Be}$ shoulder can be clearly seen at about 650 keV. Nevertheless a lot of different background sources remain in the data and cannot be rejected by coincidence analysis:

- **pp neutrinos:**

A contribution of natural ${}^{14}\text{C}$ present in the liquid scintillator is limiting the analysis of pp neutrino events. Taken into account the additional background of ${}^{85}\text{Kr}$ and ${}^{210}\text{Po}$ the analysis of pp neutrino events seems challenging at the moment.

- **CNO neutrinos:**

${}^{210}\text{Bi}$ is the mother nuclide of ${}^{210}\text{Po}$ and the important background for the CNO signal as its β decay has a shape very similar to the recoil spectrum of the CNO neutrinos. However, a large-scaled purification campaign seems to be able to reduce the distribution of ${}^{210}\text{Bi}$ inside the IV and may open the window for the analysis of CNO neutrino events in the future.

- **pep neutrinos:**

The pep signal is till now basically limited by the cosmogenic background of ${}^{11}\text{C}$ and the intrinsic background of ${}^{210}\text{Bi}$. As it will be shown in section 5.2, the TFC is a powerful technique to improve the status of the pep analysis by rejecting ${}^{11}\text{C}$ events.

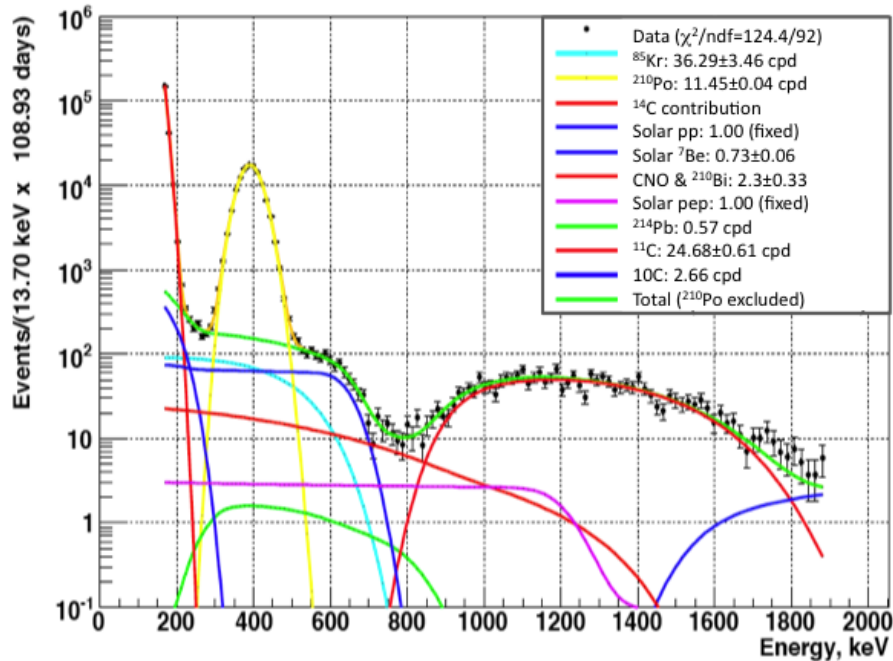


Figure 2.3: Typical BOREXINO energy spectrum (300 days measurement) with background sources and solar neutrino components. The contributions of solar pep and pp neutrinos are fixed according to the Standard Solar Model with LMA MSW oscillation solution. The solar CNO neutrino flux is fitted collectively with ^{210}Bi due to their similar spectral shape (picture taken from [27]).

2.4 Physics program and previous results of BOREXINO

With its low energy threshold of 200 keV and high radiopurity, BOREXINO has a great capability to measure all types of solar neutrinos from the low-energetic pp neutrinos to the high-energetic ^8B neutrinos. The determination of all different neutrino fluxes would not only confirm the solar model but it would also lead to constraints on the survival probability and therefore provide conclusions about the intrinsic properties of neutrinos (see section 1.2).

However, the BOREXINO collaboration is not only interested in solar neutrinos, but also in geo-neutrinos and neutrinos from supernovae. This section will give an overview on the different aspects of neutrino physics and the previous results of the BOREXINO experiment as well as the work in progress.

Solar ${}^7\text{Be}$ neutrinos

After three months of data taking the BOREXINO collaboration was able to publish the first real time measurement of the monoenergetic solar ${}^7\text{Be}$ neutrinos with an energy of 862 keV [31]. The electron recoil spectrum was clearly identified by a compton-like shoulder between 600 keV and 700 keV (see figure 2.4) after applying different basic cuts to reduce the number of background events (see section 2.3) and a statistical subtraction of the ${}^{210}\text{Po}$ α decay by α/β discrimination. The recent value of the ${}^7\text{Be}$ flux determined by BOREXINO is [32]

$$49 \pm 3_{\text{stat}} \pm 4_{\text{sys}} \text{ counts}/(\text{d} \cdot 100\text{t})$$

which is in agreement with the predictions from Standard Solar Models and the LMA-MSW neutrino oscillation theory. The next ambitious goal is to measure this rate with an total error of less than 5%.

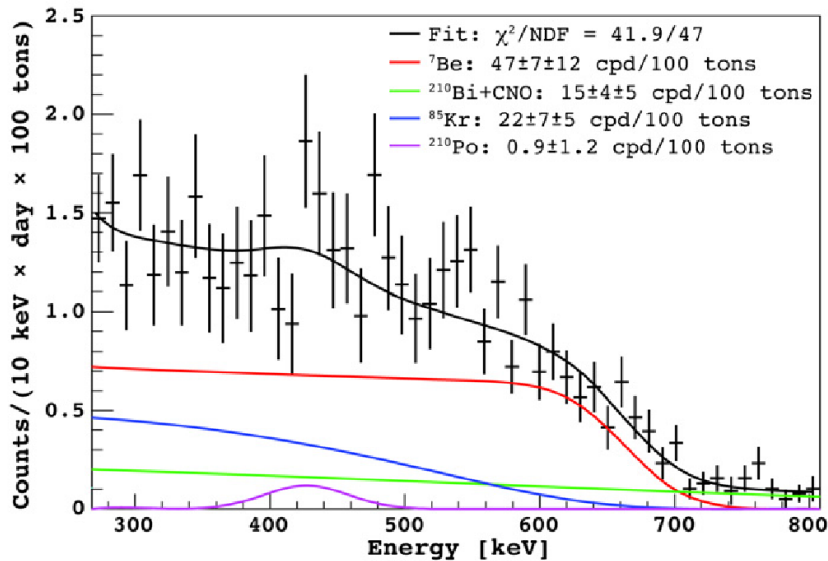


Figure 2.4: First real time detection of ${}^7\text{Be}$ solar neutrinos by BOREXINO. The energy spectrum shows the recoil of the 862 keV ${}^7\text{Be}$ solar neutrinos identified via the compton-like shoulder between 600 keV and 700 keV [31].

Solar ${}^8\text{B}$ neutrinos

In 2008, BOREXINO also detected solar neutrinos from the ${}^8\text{B}$ β^+ decay with a flux of $\Phi_{8\text{B}} = 2.4 \pm 0.4 \pm 0.1 \cdot 10^6 \text{cm}^{-2}\text{s}^{-1}$ [33]. This result is consistent with the measurements from Super-Kamiokande and SNO. As the target mass of BOREXINO

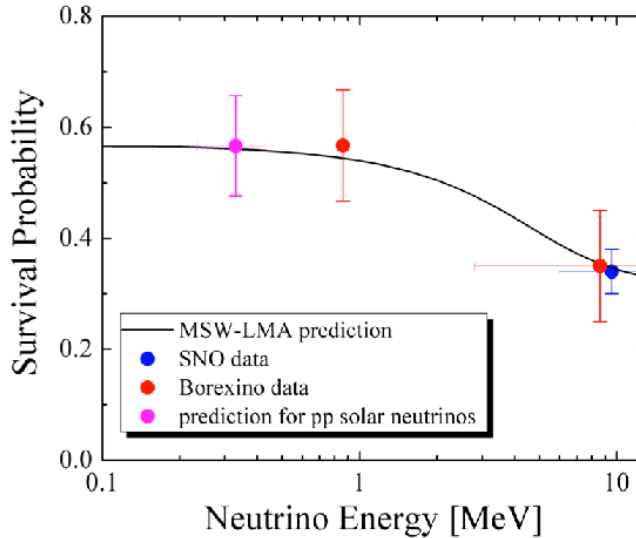


Figure 2.5: Survival probability for electron neutrinos with regard to the neutrino energy. All results concerning the results on ${}^7\text{Be}$ and ${}^8\text{B}$ neutrinos from BOREXINO and SNO are in agreement with a LMA MSW mechanism [27, 33].

is quite small compared to these water Cherenkov detectors, there is no big improvement on the ${}^8\text{B}$ rate from this point of view. However, again the low energy threshold is the advantage of the BOREXINO detector which allowed to measure these neutrinos down to 2.8 MeV, whereas the water Cherenkov detectors are limited to ~ 4 MeV.

The combination of recent results on ${}^7\text{Be}$ [32] and ${}^8\text{B}$ neutrinos from BOREXINO and SNO provide the possibility to observe the energy dependence of the survival probability for electron neutrinos (see figure 2.5). The measured solar neutrino fluxes are in agreement with the standard LMA MSW solution [33].

Geo-neutrinos

Electron anti-neutrinos emitted in a β decay from natural radioactive sources in the Earth are called geo-neutrinos. By measuring these neutrinos, it is possible to determine the composition of the Earth. This year, the BOREXINO collaboration published their first result on the rate of geo-neutrinos at the LNGS [34]. The detection channel for these anti-neutrinos is the inverse β decay which has an energy threshold of 1.8 MeV:



This reaction is identified by a delayed coincidence between the annihilation of the positron and the capture of the neutron on a proton in the scintillator ($\tau \approx 250 \mu\text{s}$), providing a very clean signal. The measured rate of geo-neutrinos in BOREXINO is $3.9_{-5.8}^{+1.6}$ events/(100 t · yr). The error of this result is too large to distinguish between different Earth composite models. However, as there is very little background for this analysis, a longer exposure time will decrease the error.

Supernova neutrinos

In case of a core-collapse Supernova at the center of the galaxy, it is expected that BOREXINO will see about 60 to 100 neutrino events. The detection will mainly depend on the inverse β decay, with small contributions from NC reactions on ^{12}C [27,35].

In 2009, BOREXINO joined the Supernova Early Warning System (SNEWS). As the neutrino signal of a Supernova is expected to arrive at the Earth several hours before the light signal, this system will be able to warn astronomers. Together with Super-Kamiokande, LVD and IceCube the neutrino detectors may also be able to reconstruct the position of the Supernova.

Chapter 3

Spectral Analysis

Despite its effectiveness for identifying radioactive background, the coincidence analysis is an impossible approach towards the search for solar neutrinos as they do not have any correlations with other events.

In Borexino, neutrinos are observed via neutrino-electron scattering, i.e. by the detection of the recoil electron in the scintillator. For this reason, neutrino events and β decay events are not distinguishable by any trigger information, but only by the difference in their spectral shapes. Therefore, neutrino spectra and the spectra of not rejected background sources have to be fitted simultaneously in a spectral analysis.

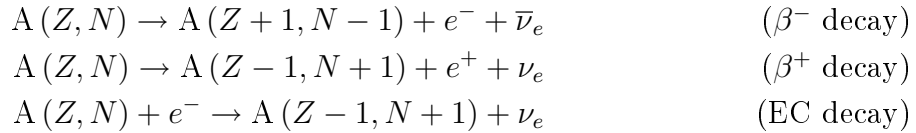
In this chapter it is shown, how the spectral analysis is accomplished. In the first and second section, the simulation of β decay spectra and the calculation of the Fermi function will be discussed. The third section treats the simulation of recoil spectra from neutrino events. Afterwards the characteristics of the detector will be taken into account to calculate the real response of the detector on the spectral shape. The last part of this chapter explains the fitting procedure which determines the rates of the respective neutrino and β spectra as well as the light yield of the detector.

3.1 Simulation of β Spectra

The β^- decay was first discovered at the beginning of the 20th century, together with the α decay and γ radiation. About 30 years later the positron, the β^+ decay and the electron capture (EC) were identified, at the same time when Fermi developed his theory of β decays [36].

3.1.1 Parameterization of allowed β Decays

In a β^\pm decay, a core bounded proton (neutron) decays into a neutron (proton) by emission of an positron (electron) and the corresponding (anti-)neutrino. Therefore, the β^+ decay is relevant for isotopes with a high proton number, whereas the β^- decay is important for isotopes with with a high neutron number. In contrast to a free proton, which is considered to be stable ($\tau > 2.1 \cdot 10^{29}$ a, 90% C.L. [1]), a free neutron undergoes coercively the β^- decay ($\tau = 885.7 \pm 0.8$ s).



The positron from the β^+ decay annihilates immediately with an electron, emitting two 511 keV γ quanta. In the EC decay, an electron of the atomic shell (usually K- or L-shell) is captured by a proton of the core which leaves a new isotope with one proton less and one neutron more than the previous element. The difference to the β^+ decay is that the EC does not have a positron in the final state, but only the neutrino.

Assuming the matrix element that is describing the transition between the initial and final state to be energy independent, the following parameterization [3] can be used to calculate the energy distribution of the electron and positron in a β decay, respectively:

$$\frac{dN}{dT} = F(Z, W) \cdot p \cdot T \cdot \sqrt{(Q - m_e - T)^2 - m_\nu^2} \cdot (Q - m_e - T) \quad (3.1)$$

The values for $\frac{dN}{dT}$ have to be read as the probability to find a number N of electrons (positrons) within an energy range dT . T stands for the kinetic energy in MeV, W for the total energy (including the rest mass) in units of $m_e c^2$ and p for the momentum in MeV/c of the emitted electron (positron). Q is the maximal energy which can occur in the decay. $F(Z, W)$ is the so-called Fermi function and describes the corrections due to the Coulomb field of the daughter nucleus (see chapter 3.2 for more information).

The electron mass is given by $m_e = 0.511$ MeV and the neutrino mass m_ν can be considered to be zero. In this case equation 3.1 simplifies to:

$$\frac{dN}{dT} = F(Z, W) \cdot p \cdot T \cdot (Q - m_e - T)^2 \quad (3.2)$$

with the same parameters introduced above. Equation 3.2 is used as basis for all spectral fits of β^\pm decays.

Figure 3.1 shows the continuous energy distribution $\frac{dN}{dT}$ for ^{11}C and ^{85}Kr . Both

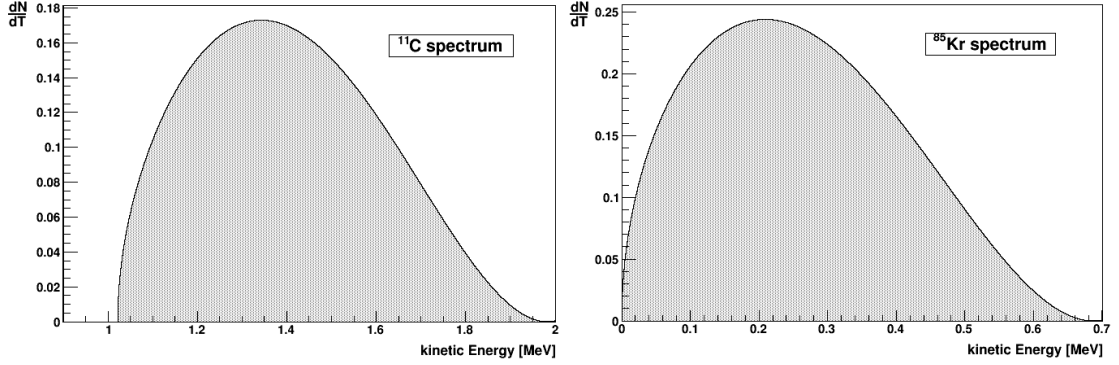


Figure 3.1: Left: Energy distribution of ¹¹C β⁺ decay. Right: Energy distribution of the ⁸⁵Kr β⁻ decay. Both spectra are calculated for $F(Z, W) = 1$ and a total number of 1000 decays for each isotope.

spectra are calculated for a constant Fermi function $F(Z, p) = 1$ and an energy binning of $dT = 0.1$ keV. Each spectrum shows a total amount of 1000 β decays. As ¹¹C undergoes the β⁺ decay, the spectrum starts at 1.022 MeV due to the electron-positron annihilation.

Regarding the shapes of the two spectra, it is notable, that they look extremely similar. A small, but not directly visible, variation of the spectral shapes is due to the different endpoints of the decays.

3.1.2 Parameterization of forbidden β Decays

For the calculation of forbidden β decays, equation 3.2 has to be modified with an energy depending shape factor $C(W)$ [37]:

$$\frac{dN}{dT} = C(W) \cdot F(Z, W) \cdot p \cdot T \cdot (Q - m_e - T)^2 \quad (3.3)$$

For the data analysis presented in this work, the first unique forbidden transition of ²¹⁰Bi and the third unique forbidden transition of ⁴⁰K will become important. The parameterization of the shape factor for both decays can be found experimentally either by linearization of the Kurie plot or using the cutoff energy yield method [37, 38]:

$$C(W) = 1 - 0.47 \cdot W + 0.065 \cdot W^2 \quad ({}^{210}\text{Bi shapefactor})$$

$$C(p, q) = p^6 + q^6 + 7 \cdot p^2 q^2 (p^2 + q^2) \quad ({}^{40}\text{K shapefactor})$$

W is the total energy of the emitted electron as stated previously, whereas p and q are the electron and the neutrino momentum, respectively.

Figure 3.2 shows the simulation of two ²¹⁰Bi spectra. The spectrum described by

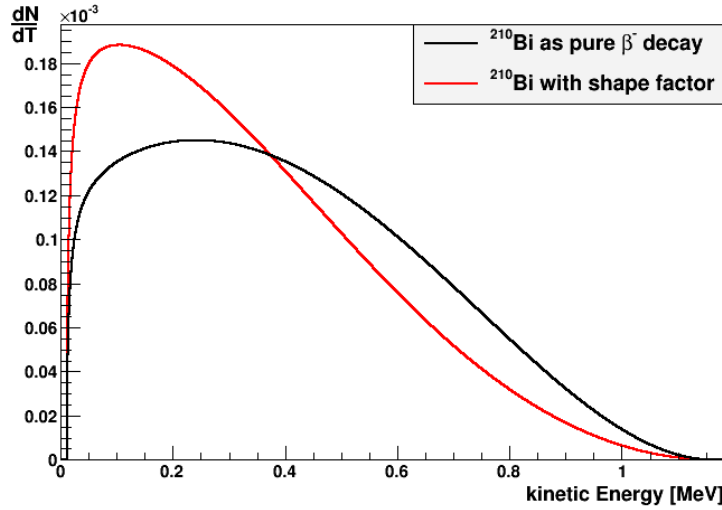


Figure 3.2: Normalized spectra of the ^{210}Bi β^- decay. Both calculations were done with $F(Z, W) = 1$. The black line represents the energy distribution assuming an allowed transition of the nucleus, whereas the red line shows the forbidden transition. The deformation of the spectrum due to the effects of the shape factor is clearly visible.

the black line corresponds to a shape factor equal to one, treating the decay of the nucleus as an allowed transition. Compared to the spectrum represented by the red line, which includes the energy depending shape factor for ^{210}Bi , the deviation in the spectral shape is clearly visible. This emphasizes the importance of the shape factor for forbidden transitions in spectral analyses.

3.2 The Fermi Function

3.2.1 Parameterization of the Fermi Function

The energy depending Fermi function $F(Z, W)$ is an additional important correction for the shape of the β -spectrum due to the Coulomb field of the daughter nucleus, which provides an attractive potential for electrons, and a repulsive potential for positrons.

Different formulas for parameterization of the Fermi function can be found in literature. For this analysis the parameterization presented in [37] is used, as it is very close to the function introduced by Fermi in his work on the theory of β

decays [36]:

$$F(\pm Z, W) = 2 \cdot (1 + \gamma) \cdot (2pR)^{2(\gamma-1)} \cdot \exp(\pi y) \frac{|\Gamma(\gamma + iy)|^2}{|\Gamma(2\gamma + 1)|^2} \quad (3.4)$$

$$\text{with } \gamma = \sqrt{1 - (\alpha Z)^2} \quad ; \quad y = \frac{\alpha Z W}{p} \quad ; \quad R = 0.5 \cdot \alpha A^{\frac{1}{3}}$$

As described in the previous section, W denotes the total energy in units of $m_e c^2$ and p the momentum of the emitted particle. Z is the proton number of the daughter nucleus. R describes the nuclear radius, depending on the mass number A of the isotope and $\alpha = \frac{1}{137}$ is the fine structure constant. The upper sign in equation 3.4 refers to the β^- , the lower sign to the β^+ decay.

$\Gamma(a + ib)$ is the gamma function defined for complex arguments. An algorithm for an implementation of this function can be found in [39].

However, besides the electrostatic effects of the daughter nucleus described by equation 3.4, the electron shell has also to be taken into account as it screens the positive charge of the nucleus. The screening effect can be estimated by shifting the Fermi function by the potential energy V_0 , which arises from the screening [37]:

$$F(\pm Z, W) \rightarrow F(\pm Z, W \mp V_0) \cdot \sqrt{\frac{(W \mp V_0)^2 - 1}{W^2 - 1}} \cdot \left(\frac{W \mp V_0}{W}\right) \quad (3.5)$$

$$V_0 \approx 1.13 \cdot \alpha^2 Z^{\frac{4}{3}} \quad (3.6)$$

Due to the square root in equation 3.5, the spectrum for β^- decays cannot be calculated over the full energy range when the screening effects are taken into account. The square root becomes negative for low kinetic energies of the electron and therefore sets a lower limit on the electron energy in the range of several keV (11.2 keV for ^{210}Bi), depending on the nucleus and leads to a systematical error in the calculated event rate. Physically, this may be interpreted as the deceleration of the emitted electrons by the screening effects of the electron shell down to such low energies, that the β^- decay cannot be observed.

Apparently, this problem is caused by using a too strongly simplified model for the calculation of the screening effects. However, the spectral fits on BOREXINO Monte Carlo data (see chapter 4) and on experimental data (see section 5.1) for different β decaying isotopes show, that they work quite well using formula 3.5.

Figure 3.3 shows the spectra of the ^{11}C β^- and the ^{85}Kr β^+ decay. The full Fermi function¹ has been applied to this calculations. Compared to figure 3.1, a distortion in the spectral shape can be seen for ^{85}Kr : As the Coulomb field provides an attractive potential the number of slow electrons is increased in the

¹The term “full Fermi function” refers within this thesis to equation 3.5, taking into account the corrections due the Coulomb field (equation 3.4) and the screening effects.

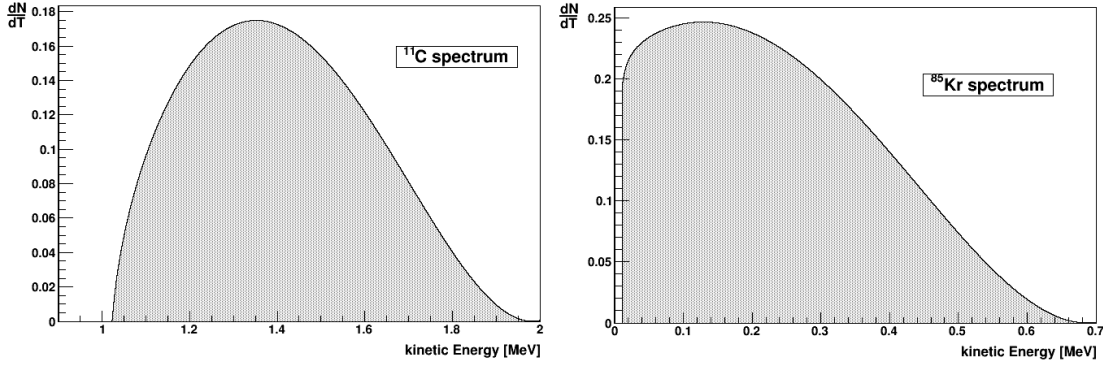


Figure 3.3: Left: Energy distribution of the ^{11}C β^+ decay. Right: Energy distribution of the ^{85}Kr β^- decay. Both spectra are calculated for a total number of 1000 decays and the full Fermi function was applied. The distortion of the spectrum compared to figure 3.1 is visible for ^{85}Kr .

energy distribution of the β^- spectrum. The fact that the deformation of the shape cannot be clearly identified for the ^{11}C spectrum emphasizes that the Fermi function becomes more important for heavy isotopes as it is also expressed by formula 3.4.

3.2.2 Comparison between Approximation and Parameterization of the Fermi function

During decades, various approximations of the Fermi function have been developed. With regards to the spectral analysis which requires the calculation of thousands of spectra (see section 3.5), it might be useful to implement a more simple parameterization than formula 3.4 to minimize the required CPU time for the spectral fits. Therefore an approximation (see equation 3.7) was compared to the parameterization introduced in the previous section. The approximation can be written as (see e.g. [40]):

$$F(\mp Z, T) \approx \frac{2\pi \cdot \eta}{1 - e^{-2\pi \cdot \eta}} \quad \text{with} \quad \eta = \frac{Z \cdot \alpha \cdot c}{v_e} \quad (3.7)$$

As before, the upper sign in equation 3.7 refers to the β^- , the lower sign to the β^+ decay. The variable v_e is the velocity of the electron or positron and c is the speed of light.

Figure 3.4 illustrates the calculated deviation between this approximation and the parameterization of the full Fermi function. It is visible, that the deviation increases for heavier isotopes. Even though the deviation for the carbon nuclide

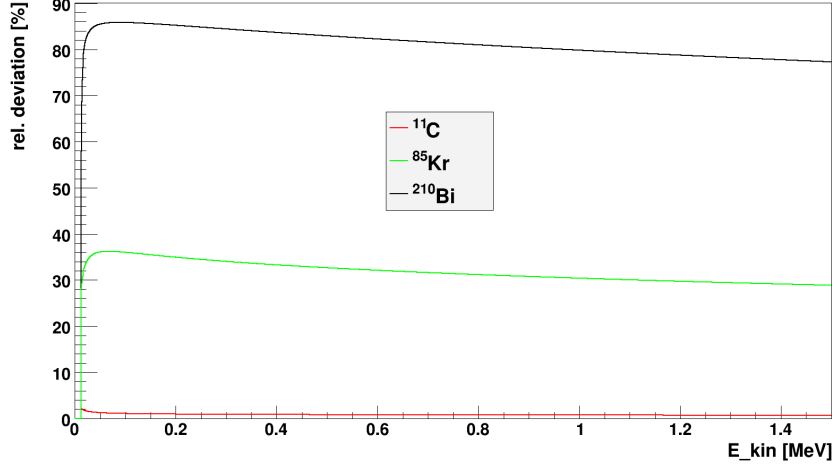


Figure 3.4: The relative deviation between the approximation and the full Fermi function given in percent. The deviation is stronger for heavier isotopes and decreases slowly with the energy of the β particle.

is quite small and is below 2%, discrepancies of more than 30% for ^{85}Kr and more than 80% for ^{210}Bi are too high to be accepted for spectral analysis. For this reason the approximation is not used for the spectral fits performed in this work.

3.3 Simulation of ν Recoil Spectra

The signal of neutrinos detected via neutrino-electron scattering is created by the energy deposition of the recoil electron. The kinetic energy T of this electron depends on the neutrino energy E as well as on the scattering angle ϕ and can be calculated analog to the energy distribution of the compton scattering:

$$T = E - \frac{E}{1 + \frac{E}{m_e c^2} (1 - \cos(\phi))} \quad (3.8)$$

The recoil spectrum of the electron can then be calculated to [41]:

$$\frac{dN}{dT} = \int_{E_{min}}^{E_{max}} \left(\frac{d\sigma_{\nu_e e}}{dT}(E, T) \cdot \langle P_{\nu_e \rightarrow \nu_e} \rangle + \frac{d\sigma_{\nu_{\mu} e}}{dT}(E, T) \cdot (1 - \langle P_{\nu_e \rightarrow \nu_e} \rangle) \right) \cdot \lambda_{\nu_e}(E) \cdot dE \quad (3.9)$$

As stated in section 1.2.1 the effects of the third neutrino flavor can be neglected for solar neutrinos and a two-flavor approximation is applied.

In this work the only considered solar neutrinos are the monoenergetic ^7Be and

pep neutrinos. Therefore the emission spectrum of the neutrinos from the sun $\lambda_{\nu_e}(E)$ is a delta function at the corresponding neutrino energies. As input for the averaged survival probability $\langle P_{\nu_e \rightarrow \nu_e} \rangle$ the result for the MSW LMA solution (averaged over day and night) evaluated by J. N. Bahcall [42] is used.

$\frac{d\sigma_{\nu_x e}}{dT}(E, T)$ denotes the differential cross section for neutrino-electron scattering [43, 7]:

$$\frac{d\sigma_{\nu_x e}}{dT}(E, T) = \frac{2G_F m_e^2}{\pi \hbar^4} \left(g_L^2 + g_R^2 \left(1 - \frac{T}{E}\right)^2 - g_L g_R \left(\frac{T \cdot m_e}{E^2}\right) \right) \quad (3.10)$$

$$\text{with} \quad g_L = \sin^2(\theta_W) \pm \frac{1}{2} \quad g_R = \sin^2(\theta_W) \quad (3.11)$$

The upper sign in equation 3.11 refers to the scattering of electron neutrinos and the lower sign to the scattering of the muon neutrinos. θ_W is the so-called Weinberg angle (weak mixing angle) with $\sin^2(\theta_W) = 0.231$ and G_F the Fermi coupling constant.

Figure 3.5 shows the calculated recoil spectrum for the ${}^7\text{Be}$ solar neutrinos with 862 keV energy and a total of 1500 events. The maximal kinetic energy for a recoil electron is 665 keV with a scattering angle of 180° . The compton like shoulder lies sharply at the maximal energy.

3.4 Calculation of the Detecor response

All spectra shown in the previous section would be valid, if the energy resolution of the detector would be perfect and the total deposited energy could be measured. However, quenching effects cause a loss of visible energy and the detector resolution softens the spectral shapes. Therefore it is necessary to take these characteristics of the detector into account.

3.4.1 Quenching Effects

A particle travelling through the detector excites the molecules of the liquid scintillator. The molecules emits a part of this energy in form of scintillation light, but a small percentage of the energy can be lost in radiaonless deexcitation modes. These so-called energy quenching processes are depending on the nature of the particle and can be described by the Birks function [44]. By calibrating the detector with different radioactive sources of well known energy, it is possible to find an

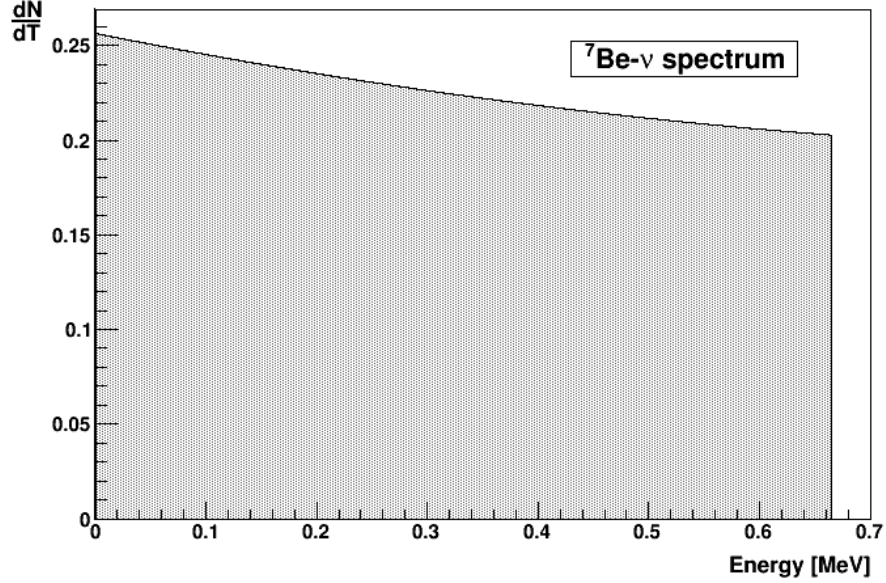


Figure 3.5: The electron recoil spectrum of the ${}^7\text{Be}$ solar neutrinos with 862 keV energy. The compton like shoulder lies at 665 keV according to a scattering angle of 180° .

empirical function for the quenching effects, valid for the BOREXINO detector [41]:

$$f(T) = 1 - \frac{1}{\left(1 + \frac{T}{0.002186 \text{ MeV}}\right)^{0.4986}} \quad (\text{e}^\pm \text{ quenching})$$

$$f(T) = 1 - \frac{1}{\left(1 + \frac{T}{0.746 \text{ MeV}}\right)^{3.892}} \quad (\gamma \text{ quenching})$$

whereas $f(T)$ is the fraction of the deposited energy T emitted as scintillation light.

In BOREXINO the measured energy of an event is described by different ECHIDNA variables. The variable used throughout this work for the spectral fits is *charge* (see section 2.2). This variable provides the energy in units of photoelectrons (p.e.) collected by the PMTs. The deposited energy T given in MeV can easily be expressed as deposited charge q in p.e. with the light yield (LY) as conversion factor:

$$q [\text{p.e.}] = LY \cdot f(T) \cdot T [\text{MeV}] \quad (3.12)$$

For the BOREXINO detector, the effective light yield is approximately $500 \frac{\text{p.e.}}{\text{MeV}}$ [24]. In spectral analysed it is left as a free parameter.

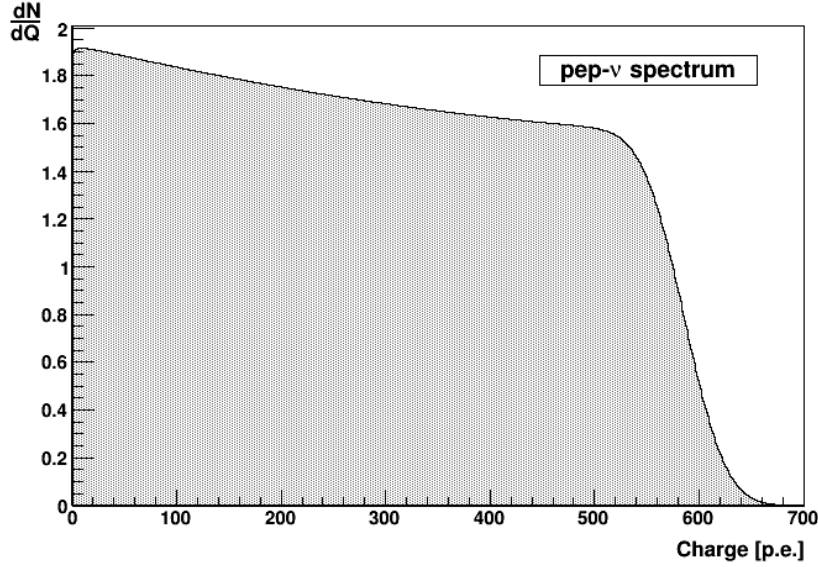


Figure 3.6: The electron recoil spectrum of 1000 pep solar neutrino events with 1.442 MeV energy, calculated with $LY = 500 \frac{\text{p.e.}}{\text{MeV}}$. The effect of the energy resolution can be seen in the softening of the compton shoulder.

3.4.2 Energy Resolution

The response function $R(Q, q)$ of the detector defining the energy resolution can be determined by fitting the ^{210}Po peak. It depends on the visible charge Q and the deposited charge q in the detector and is similar a gaussian distribution:

$$R(Q, q) = \frac{1}{2\pi \cdot \sigma} e^{-\frac{1}{2} \left(\frac{Q-q}{\sigma} \right)^2} \quad (3.13)$$

σ is the statistical error given as $\sigma = \sqrt{q}$.

The calculated energy spectrum $\frac{dN}{dT}$ must be convolved with the response function to get the spectrum of the visible charge in BOREXINO:

$$\frac{dN}{dQ} = \int_0^{E_{max}} R(Q, q) \cdot \frac{dN}{dT} \cdot dT \quad (3.14)$$

Figure 3.6 shows the electron recoil spectrum for solar pep neutrinos. The maximal kinetic energy of a recoil electron can be ~ 1.225 MeV which corresponds to ~ 586 p.e. with a light yield of $500 \frac{\text{p.e.}}{\text{MeV}}$. Compared to the sharp compton like edge in figure 3.5 the influence of the detector's energy resolution softens the shoulder of the spectrum.

3.5 The χ^2 Fitting Procedure

To determine the compatibility between data and the calculated spectra, the method of least squares is applied. Therefore the spectra are fitted to each other by comparing them bin by bin. The χ^2 value calculated over all bin numbers i

$$\chi^2 = \sum_i \left(\frac{N_i^{exp}(Q) - N_i^{th}(Q)}{\sigma_i} \right)^2 \quad (3.15)$$

describes the deviation between these spectra. N_i^{exp} is the entry in bin number i for the experimental (data) spectrum and N_i^{th} for the theoretical (calculated) spectrum, respectively, whereas $\sigma_i = \sqrt{N_i^{exp}(Q)}$ denotes the statistical error of the respective bin.

The experimental data sample is reproduced best by the spectrum with the lowest χ^2 value. To find this spectrum, it is necessary to vary the free parameters of the fit, the light yield and event rate of the respective background and solar neutrino sources, in broad ranges and small steps. This can result in more than 50.000 spectra which have to be calculated for one spectral fit, considering an interval of $50 \frac{\text{p.e.}}{\text{MeV}}$ for the light yield and 1000 events for the rate, varied in steps of $1 \frac{\text{p.e.}}{\text{MeV}}$ and one event.

The χ^2 probability density function (p.d.f.) is defined by [1]

$$f(z; n) = \frac{z^{\frac{n}{2}-1} \cdot e^{-\frac{z}{2}}}{2^{\frac{n}{2}} \cdot \Gamma\left(\frac{n}{2}\right)} \quad \text{with} \quad z \geq 0 \quad (3.16)$$

where n denotes the number of free parameters in the spectral fit.

To evaluate the error range for the free parameters of the fit within a given confidence level, the so-called critical value m has to be calculated by integrating the χ^2 p.d.f.:²

$$P = \int_0^m f(z; n) \cdot dz \quad (3.17)$$

For a confidence level of 90%, corresponding to $P = 0.90$, and a fit with two free parameters (LY and rate), the critical value is $m = 4.61$. The error range of the parameters is then given by the interval $[\chi_{min}^2 - m; \chi_{min}^2 + m]$.

Usually not the minimal χ^2 , but the normalized value is cited: $\frac{\chi^2}{ndf}$, with ndf the number of degrees of freedom. In spectral analysis, the ndf is the number of fitted bins less the number of free parameters. If the deviation between the fitted spectra is only due to statistical effects and not to a systematic discrepancy, $\frac{\chi^2}{ndf}$ is expected to be close to one.

² The evaluation of the integral in equation 3.17 was done using the Wolfram Mathematica Online Integrator [45].

Chapter 4

Spectral Fits on BOREXINO Monte Carlo Data

Before the procedure of spectral analysis (see chapter 3) can be applied to the search for solar pep neutrinos in BOREXINO data, the approach to spectral fits and its implementation has to be validated. Therefore it is reasonable to test the procedure at first on clean data sample with only one background or neutrino source. However, only few background sources can be prepared by means of coincidence analysis with sufficient purity and statistics (e.g. ^{11}C , see section 5.1), the first tests were done on Monte Carlo (MC) data.

The BOREXINO Monte Carlo (BXMC) is based on Geant4, a toolkit for the simulation of particle reactions with matter used in high energy, accelerator and nuclear physics [46]. It includes the setup of the detector as well as the characteristics of all material and fluids and is organized in different modules. The modules used to simulate the following data spectra are the *RDM* (Radioactive Decay Module), *SCS* (Special Cross Section generator) and *SolarNeutrino* module.

The *RDM* provides the decay of radioactive isotopes inside the detector using the *G4IonTable*. It was used to simulate the ^{11}C and ^{85}Kr energy spectrum, which will be shown in the first part of this chapter. As the *RDM* does not take the shape factor correction for forbidden β decays into account, the ^{210}Bi spectrum is generated with the *SCS* module, where the decay of this isotope is implemented without referring to the ion table. The neutrino spectra in the second part of this chapter were created by the *SolarNeutrino* module.

4.1 Fits on Background Sources

This section treats the spectral fits of different β decays which are background sources for the solar neutrino search. All data samples were generated by the BXMC within the FV. Every fit has two free parameters: The light yield and the total rate of the decay. These parameters are scanned in steps of $1 \frac{\text{p.e.}}{\text{MeV}}$ and 1 event, respectively. If not stated otherwise, all given statistical errors are estimated for a 68.27% confidence level.

4.1.1 ^{11}C Spectrum

The cosmogenic isotope ^{11}C is produced in the FV of the detector when a neutron is knocked off a ^{12}C atom in the liquid scintillator:



It undergoes the β^+ decay with a half life of $T_{\frac{1}{2}} = 20.38$ min and an endpoint of 0.96 MeV. As stated in section 2.3 the ^{11}C background is extremely important for the search for solar pep neutrinos as the expected shoulder of the pep recoil signal is expected at the same energy range as the peak of the ^{11}C decay.

The black crosses in figure 4.1 are the data points of the simulated MC spectrum, at which the vertical line indicates the statistical error of the respective energy bin. The energy drawn on the x-axis is given as the *charge* in p.e., normalized to 2000 living PMTs, with a binning of 10 p.e. The red spectrum is the calculated best fit of the β^+ energy distribution.

The fit was done in the energy region between 420 p.e. and 820 p.e. and returns as minimal χ^2 value $\frac{\chi^2}{ndf} = 1.13$. This best fit was generated using a light yield of $478 \pm 1 \frac{\text{p.e.}}{\text{MeV}}$ and a rate of 4900 ± 108 events which has to be compared to the expected rate of 4983 events. This result demonstrates, that the fitting procedure for the β^+ decay works very well.

Due to the annihilation of the positron of the β^+ decay with an electron, the ^{11}C spectrum is shifted to an energy of 1.022 MeV, which corresponds to 380 p.e. including the effects of the γ quenching. It appears that the MC is based on a different formula for this quenching than the spectral analysis (see section 3.4.1), as the fit result for the light yield is noticeable lower than in the following fits. This topic will be discussed in more detail in section 5.3.

4.1.2 ^{85}Kr Spectrum

The radioactive isotope ^{85}Kr is a component of the air and an intrinsic background in BOREXINO. The β^- decay to ^{85}Rb can occur via two transitions. The first transition has a half life of $T_{\frac{1}{2}} = 4.48$ h and is unimportant considering the lifetime

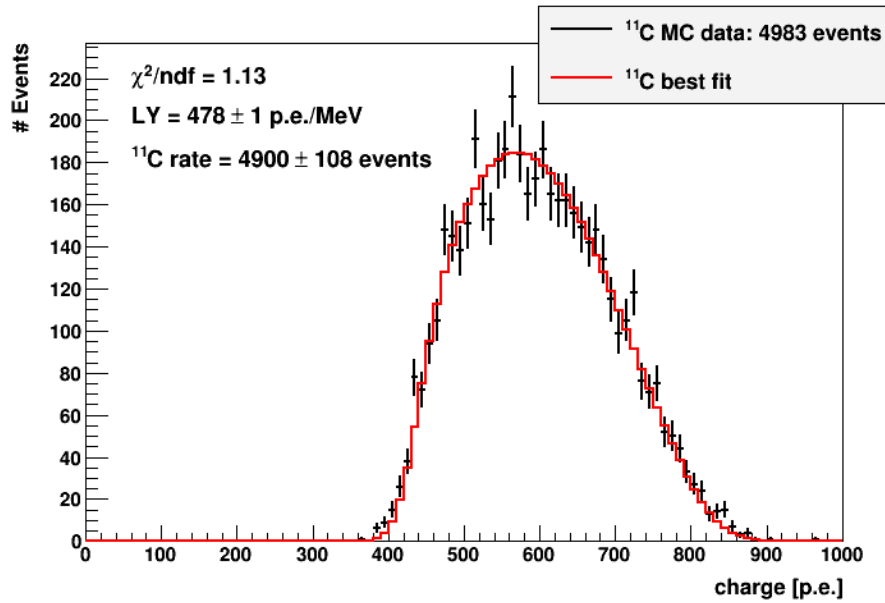


Figure 4.1: Spectral fit of the β^+ spectrum of ^{11}C . The data (black) simulated with BXMC is well reproduced by the red β^+ spectrum with $\text{LY} = 478 \frac{\text{p.e.}}{\text{MeV}}$ and a rate of 4900 events.

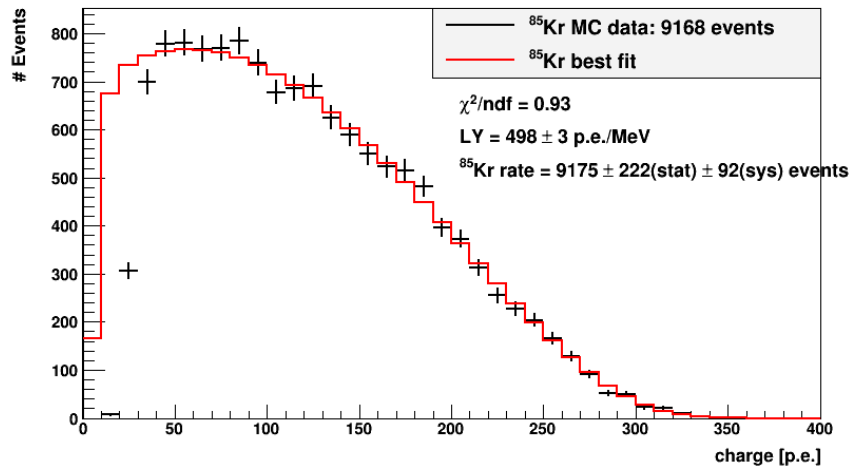


Figure 4.2: Spectral fit of a β^- spectrum of ^{85}Kr . The numerical results of this analysis for the light yield and the event rate are very good.

of the detector. The other decay provides a half life of $T_{\frac{1}{2}} = 10.76$ a and an endpoint of 0.687 MeV.

In figure 4.2 as well as in the following MC spectra, the data breaks off for energies below ~ 60 p.e. due to the energy threshold of the detector, which results in a lower limit for the fit range. Therefore, the spectrum was fitted between 70 p.e. and 310 p.e. The result of this spectral analysis shows a very good agreement between the MC data and the calculated β^- spectrum. The shape of the energy distribution and the expected values for the light yield and the event rate were reproduced very well.

As the fitted spectrum was calculated including the screening effects of the electron shell, there is a systematic error on the event rate (see section 3.2.1). It was estimated to approximately 1% by calculating the percentage of the rate below the energy threshold for which the screening effects cannot be taken into account for this β^- decay. This had to be done using a β^- spectrum of ^{85}Kr calculated with the Fermi function only including the Coulomb correction due to the electric field of the daughter nucleus. However, this procedure is a very rough approach to determine the systematic error because the spectral shape of a spectrum including the screening effects does not necessarily equal the spectrum taking into account only the effects of the nucleus. Therefore the result can only be interpreted as an estimation of the order of magnitude for this systematical error.

4.1.3 ^{210}Bi Spectrum

The intrinsic contamination of the detector with ^{210}Bi originates from the uranium chain as a natural radioactive source. The β^- decay of ^{210}Bi to ^{210}Po has a half life of $T_{\frac{1}{2}} = 5.013$ d and the energy spectrum of the electrons ends at 1.163 MeV. Therefore the energy range of this decay is similar to the expected recoil signal of the CNO neutrinos and forms an almost as significant background for the pep neutrino signal as the ^{11}C distribution.

Figure 4.3 shows the fit of a ^{210}Bi spectrum including the shape correction for the first unique forbidden transition. The spectral fit was applied from 100 p.e. up to 520 p.e. The result seems reasonable with regard to normalized χ^2 value and the fitted event rate. However, an exceptional high light yield was found for this fit, even though, the given value for the light yield in the MC code was the same as for all other spectra, β spectra as well as ν spectra. Thus it is expected to be between $470 \frac{\text{p.e.}}{\text{MeV}}$ and $500 \frac{\text{p.e.}}{\text{MeV}}$. Furthermore, a discrepancy in the spectral shape between the MC data and the calculated β spectrum is visible for less than 100 p.e. which cannot be explained by statistical fluctuations.

To identify the source of these deviations, a second fit on a ^{210}Bi spectrum was performed within the same fit range, which is shown in figure 4.4. This time the MC data was simulated with the BXMC *RDM* module not including corrections

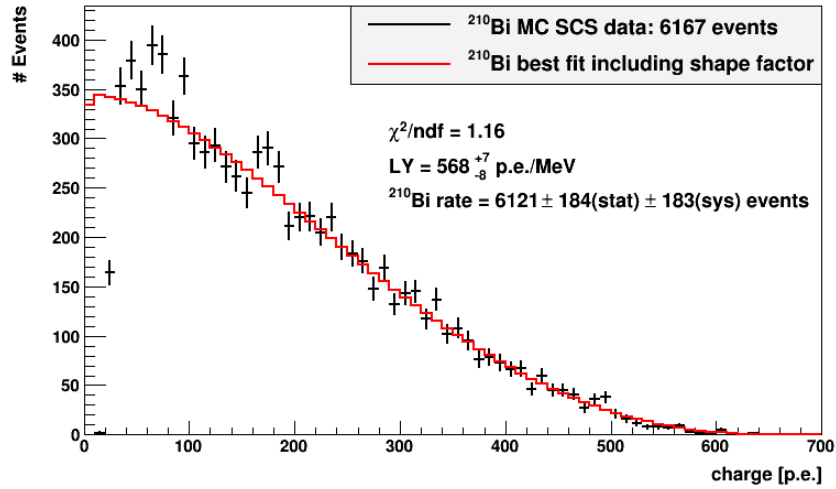


Figure 4.3: Spectral fit of a β^- spectrum of ^{210}Bi including the shape factor.. Noticeable are the exceeding high light yield favoured by the fit and the discrepancy between the fit and the MC spectrum below 100 p.e.

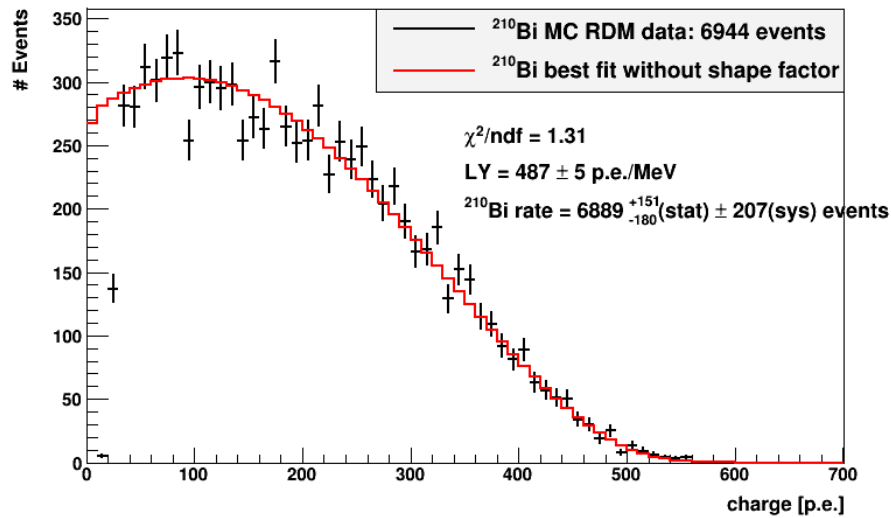


Figure 4.4: Spectral fit of a β^- spectrum ^{210}Bi without shape factor.. The spectral shape of the MC spectrum was reproduced well with regard to statistical fluctuations and the numerical fit results are satisfying.

from the shape factor. As the ^{11}C and the ^{85}Kr spectrum before, the spectrum of the ^{210}Bi decay could be reproduced without significant deviations in the spectral shape and the fit returns satisfying results for the light yield and event rate.

Thus, the discrepancy observed in the fit of the first data sample is connected to a different implementation of the shape factor in the procedure for the spectral analysis (see section 3.1.2) and in the Monte Carlo source code of the *SCS* module. This topic is currently under investigation as it will be of great importance for future spectral analysis, particularly concerning the search for CNO neutrinos. However, it can be stated, that in both cases the spectral shape was reproduced very well for energies above 300 p.e. As the performed spectral analysis for the determination of the pep neutrino rate in BOREXINO data (see section 5.2) does not include lower energies, it was decided to use for this fit the shape factor implemented in the spectral analysis (see section 3.1.2).

The calculated event rate of the ^{210}Bi β^- decay has a systematic error of approximately 2% when the screening effects of the electron shell are taken into account (see section 3.2.1). The value of this error was estimated using the same method as explained in section 4.1.2. This error can be avoided by only calculating the effects of the nucleus (equation 3.4) resulting in an inaccuracy of the spectral shape which also leads to a systematic error in the event rate. However, this error due to the neglect of screening effects can be determined quite precisely by direct comparison of two β^- spectra of ^{210}Bi , one including screening effects and the other neglecting them. This was done for energies above 600 keV, which is the important energy region for the fit on experimental data determining the pep neutrino rate (section 5.2). It was found to be 3%.

As a systematic error is unavoidable in the calculation of the ^{210}Bi spectrum, whether the screening effects are included or not, and the order of magnitude for this error is the same in both options, it was decided to neglect screening effects for this isotope in this work because it is possible to determine the resulting error more precisely compared to the first case.

With regard to the identification of pep ν events it is important to investigate a possible correlation between the ^{210}Bi and pep ν rate for determining the error propagation of the systematic error. However, as long as the origin of the detected deviations in the ^{210}Bi spectrum is not completely clarified, such an analysis based on MC data is not practicable.

4.2 Fits of Solar Neutrino Spectra

The energy distribution of the two monoenergetic solar neutrino sources were simulated with the same basic conditions as the β spectra presented in the previous section. This includes the homogeneous distribution of the neutrino events within the FV as well as the scanning of the light yield and the event rate during the spectral analysis.

4.2.1 ${}^7\text{Be}$ - ν Spectrum

As explained in section 1.3.1 the EC decay of ${}^7\text{Be}$ leads to an excited state of ${}^7\text{Li}$ in 10.3% of all decays. Therefore, there are two neutrino lines occurring from ${}^7\text{Be}$ at two different energies: 0.862 MeV and 0.384 MeV. However, it can be seen in figure 4.5 that the low-energetic signal is hardly present in the MC data due to the threshold effect of the detector.

The spectral fit was applied in the energy region between 100 p.e. and 340 p.e. Judged by the value of the normalized χ^2 , the fit of the ${}^7\text{Be}$ MC spectrum is not as well as the fits of the β spectra of ${}^{11}\text{C}$ and ${}^{85}\text{Kr}$. Despite the strong fluctuations of the MC data, the spectral analysis returns good results for the event rate and the light yield.

4.2.2 The pep- ν Spectrum

After the successful detection of ${}^7\text{Be}$ and ${}^8\text{B}$ neutrinos, The real-time measurement of the pep- ν signal at 1.442 MeV is one of the next goals of BOREXINO and the main task of this work.

Figure 4.6 shows the fit of a MC spectrum with 3240 pep neutrino events between 100 p.e. and 600 p.e. The result of this fit is very good with regard to the determination of the event rate, which is exceptional close to the expected rate of the MC data, with only $\sim 0.4\%$ deviation.

This fit clearly demonstrates the great potential of the spectral analysis.

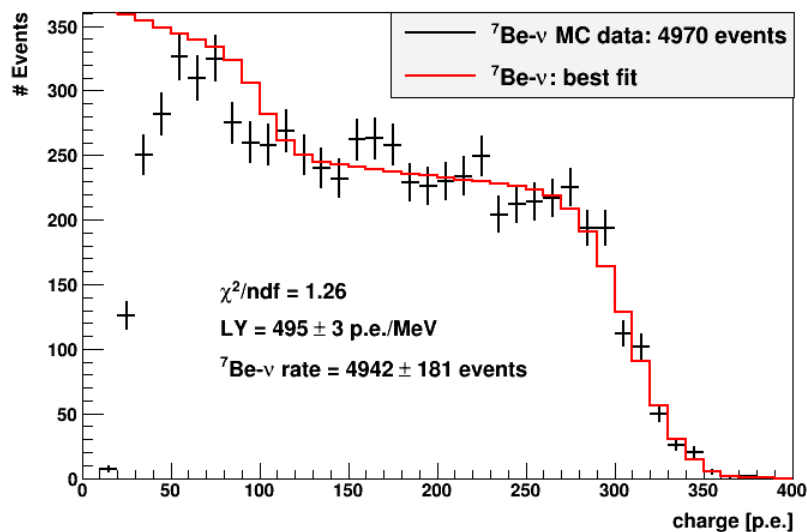


Figure 4.5: Spectral fit of the electron recoil spectrum of solar ${}^7\text{Be}$ neutrinos. The low-energetic neutrino signal is almost completely invisible in the MC spectrum due to threshold effects. Considering the statistical fluctuations of the data set, the results of the fit are quite good.

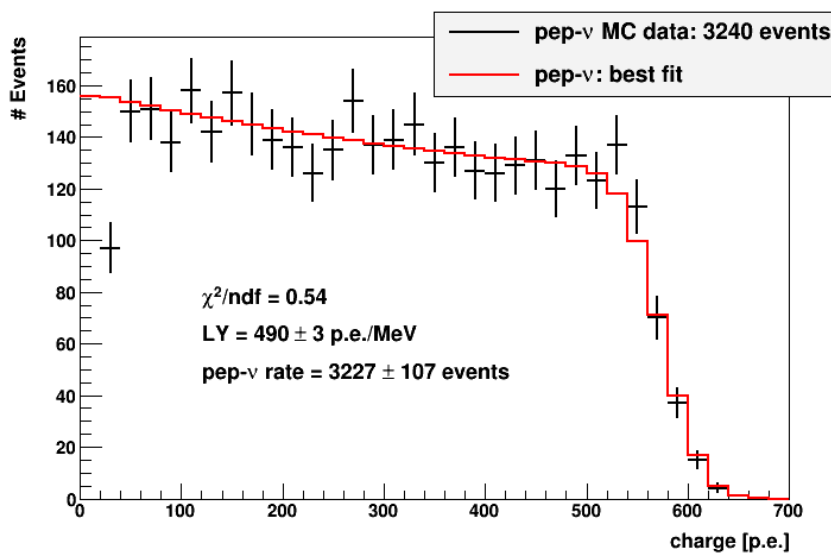


Figure 4.6: Spectral fit of the electron recoil spectrum of solar pep neutrinos.. The shape of the MC spectrum and the event rate were reproduced at a very high precision.

Chapter 5

Spectral Fits on Experimental Data of the BOREXINO Experiment

In the previous chapter the implemented spectral analysis was validated on Monte Carlo (MC) data. The next step is the application of this method on BOREXINO data with the goal to identify the solar pep neutrino signal. Therefore, the main part of this chapter treats the combined fit of background and neutrino sources of a measured BOREXINO data sample with 633.82 d of detector life time with a free contingent of pep neutrino events (section 5.2).

However, before presenting the results of this spectral analysis, the first part of this chapter shows a fit of a ^{11}C spectrum which was extracted from BOREXINO data by the Three-Fold Coincidence (TFC) technique. This fit provides a crosscheck on the goodness of the fitting procedure on real data.

At the end of the chapter, an upper limit on the amount of the primordial isotope ^{40}K in the BOREXINO data is determined and its influence on the pep neutrino signal is investigated.

5.1 Fit on ^{11}C Spectrum selected by TFC

The black data points in figure 5.1 represent events in the detector which were tagged as β^+ decays of ^{11}C by means of the TFC technique during a detector life time of 392.79 d [47]. The data selection includes a muon cut by the Outer Detector (OD) using the *trigger.btb_inputs* variable as well as a cut to the Fiducial Volume (FV) with 3.021 m radius, corresponding to a target mass of 100 t (see section 2.2). The TFC method was applied on this data sample with a time window between 2.4 min and 30 min for the ^{11}C candidate and within a radius of 1 m with regard to the neutron. As the first 2.4 minutes after the neutron event are rejected, the data sample was effectively cleaned of the cosmogenic isotope ^{10}C . All cuts together provide a ^{11}C data sample with a purity of 95% [47]. The remaining 5% of the

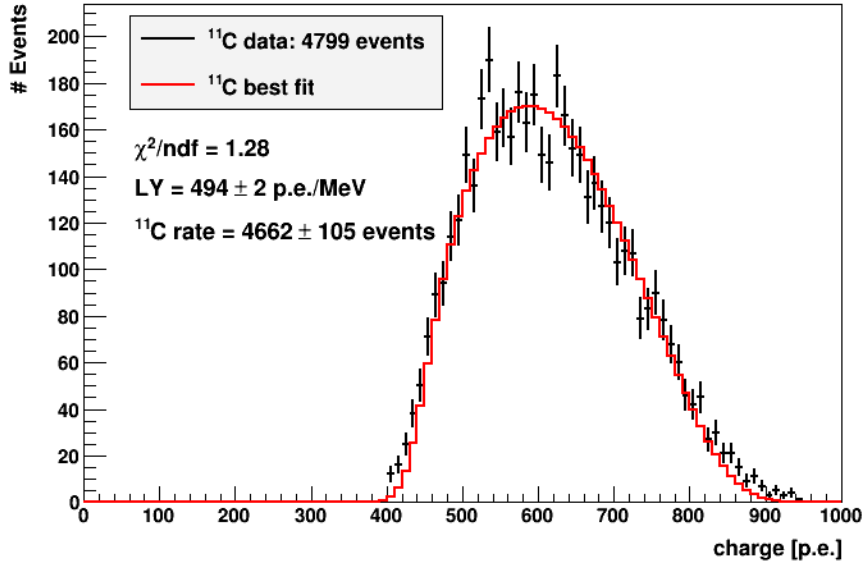


Figure 5.1: Spectral fit of a ^{11}C spectrum selected from BOREXINO data by the TFC method. The fit of this spectrum could not reproduce the event rate of ^{11}C decays within the 68.27% confidence level due to a contamination of $\sim 5\%$ of the data with muon events and external γ background.

data are remaining muon events and external γ radiation.

The values concerning the light yield and the total event rate were scanned in steps of $1 \frac{\text{p.e.}}{\text{MeV}}$ and 1 event, respectively. The fit between 450 p.e. and 850 p.e. returns a normalized χ^2 of 1.28 which is slightly higher compared to the fit on MC data (see section 4.1.1). However, the calculated light yield is consistent with the expected value of about $500 \frac{\text{p.e.}}{\text{MeV}}$ and the determined event rate provides $(97 \pm 2)\%$ of the total event number contained in the data sample, which is in agreement with the expected purity of the data sample in ^{11}C .

5.2 Combined Spectral Fit of Background and Neutrino Sources

This section summarizes the fitting procedure applied on a BOREXINO data sample with 633.82 d of detector life time and its results. The first part is devoted to the data selection and the applied software cuts to reject the majority of background events. The second part presents the execution of the fit and the first result on the solar pep neutrino rate.

5.2.1 Data Selection

In order to extract a low background energy spectrum from the BOREXINO data the following cuts were performed (see section 2.2):

- Muon events were identified by the OD using the *trigger.btb_inputs* and in addition by a combination of *mean_time*, *peak_times* and *nhits* selection.
- The fast muon daughters were rejected by a 2 ms time cut following the muon.
- Background events from fast coincidences were eliminated via the *phystag* variable (see section 2.3).
- The cosmogenic background from ^{11}C and ^{10}C was reduced using the TFC method (see section 2.3). The chosen time window and spatial distribution was 1.5 h and a radius of 2 m with regard to the neutron capture position.
- The *laben.clusters.charge* variable was normalized to 2000 living PMTs. To avoid contamination from ^{14}C and ^{210}Po , the lower limit for the energy was set to 300 p.e., which corresponds to about 600 keV.

Apart from these cuts, in a first radial cut all events outside the FV of 3.021m were neglected to reduce the number of background events from external γ radiation. Figure 5.2 shows the radial distribution of all remaining events with less than 800 p.e., corresponding to about 1.6 MeV, within the selected data sample. Events with a higher energy were not considered, as they are unimportant within the energy window of the expected pep neutrino signal.

As the external background has to decrease exponentially with regard to the radius, it can be distinguished from the homogeneously distributed internal background and neutrino signal. Therefore, the total radial distribution is described by the sum of a constant and an exponential term:

$$f(r) = (a + A \cdot e^{\lambda r}) \cdot r^2 \quad (5.1)$$

The additional factor r^2 is due to the spherical symmetry of the detector. With the result of this fit shown in figure 5.2, it is possible to calculate the percentage of events related to external γ radiation at a certain radius. As it can be seen, the external γ contamination for a FV with 3.021 m radius is still 53.9%. For a FV of 1.8 m, it was found to be 3.8%. This number refers to the energy range between 300 p.e. and 800 p.e. giving an estimation of the amount of external background in the pep- ν energy window.

It was not possible to eliminate the external background any further, as the reduction of the FV below 1.8 m would not leave enough statistic for a spectral analysis.

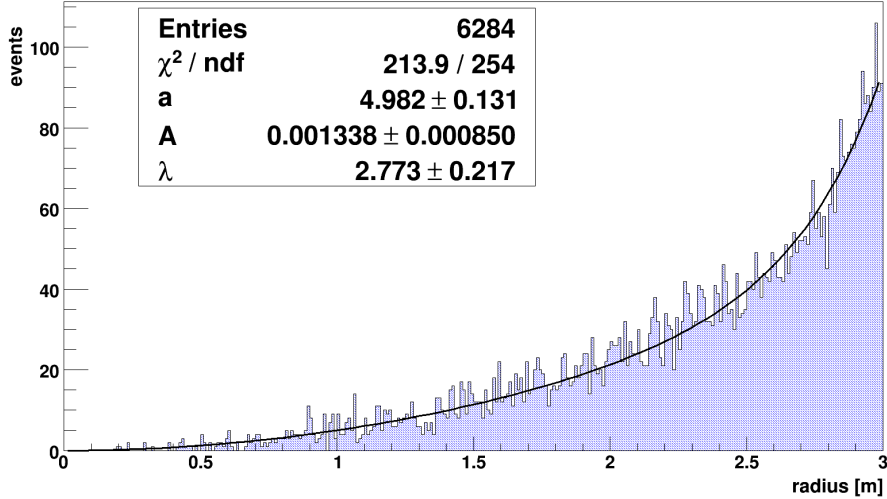


Figure 5.2: Radial distribution of the selected events within the FV. The fit function (equation 5.1) includes a quadratic and an exponential term to determine the fraction of external background events after the FV cut.

Therefore, a FV cut with 1.8 m was chosen.

The selected data sample covers the period from 15th of December 2007 to 15th of May 2010. The life time of the detector within this time limit is reduced due to time depending cuts, which are used for example in the TFC method. The effective life time was determined by applying the same cuts which were used for extracting the data sample on the energy region between 175 p.e. and 225 p.e. where the peak of the α decay of the ^{210}Po contamination is located. By comparing the amount of ^{210}Po events before and after the cuts were applied, the effective life time of the detector for this data sample was calculated to 633.82 d.

5.2.2 Spectral Analysis with free contingent of pep ν events

The energy spectrum of the selected data sample (black data points) is shown in figure 5.3 together with the results of the spectral analysis for a charge binning of 25 p.e.

The energy region most sensitive to the pep ν signal is between 500 p.e. and 650 p.e., which features the compton-like shoulder of the pep neutrino signal. All background sources contributing in this energy range have to be determined as well to reduce systematic errors in the pep neutrino rate. Thus the fit was done for an energy range between 325 p.e. and 825 p.e. By expanding the fit range, it becomes necessary to take solar ^7Be ν events into account, too.

As in all previous fits, the light yield was scanned in steps of $1 \frac{\text{p.e.}}{\text{MeV}}$ and all rates

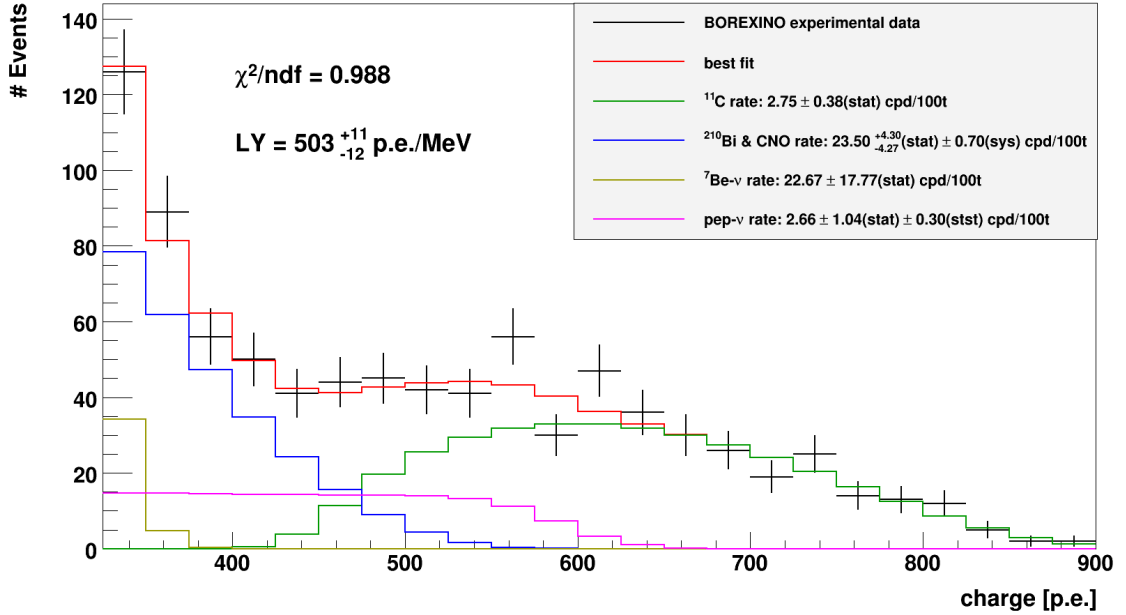


Figure 5.3: Spectral fit on experimental data with 633.82 d of detector life time with a free pep ν contingent. All given statistical errors are calculated for 68.27% confidence level. The determined signal of solar pep ν events has a statistical significance of 99.998%.

in steps of 1 event, corresponding to $\sim 7.5 \cdot 10^{-3}$ cpd/100t.

The results of this spectral analysis are illustrated in figure 5.3. According to the normalized χ^2 value of 0.988 the data sample can be described very well by the assumed β decay backgrounds and neutrino sources. Furthermore, the fitted value for the light yield is in good agreement with the expected number of $\sim 500 \frac{\text{p.e.}}{\text{MeV}}$. Table 5.1 summarizes the determined values for the light yield of the detector and the rates of the considered sources. The systematic error due to the calculation of the FV was neglected. The rates of the β decaying isotopes ^{11}C and ^{210}Bi as well as the rate for solar ^7Be ν events are compared with the results of the recent ^7Be analysis of BOREXINO [32]. Regarding the number of counts related to the cosmogenic ^{11}C background it can be seen that the TFC method almost decreased this rate in a factor of ten and leaving it in the same order of magnitude as the expected pep ν signal.

The identification of the ^{210}Bi and solar CNO ν event rate is based on the assumption, that both contributions have the same spectral shape (see section 2.3). Therefore they were fitted collectively with one parameter. As described in section 4.1.3 the neglect of screening effects for ^{210}Bi leads to a systematical error of 3%.

Parameter	Fitted value	Expected value
LY	$503_{-12}^{+11}(\text{stat}) \frac{\text{p.e.}}{\text{MeV}}$	$\approx 500 \frac{\text{p.e.}}{\text{MeV}}$
^{11}C	$2.75 \pm 0.38(\text{stat}) \text{ cpd}/100\text{t}$ after TFC cut	$25 \pm 1 \text{ cpd}/100\text{t}$ without TFC cut
^{210}Bi & CNO ν	$23.50_{-4.27}^{+4.30}(\text{stat}) \pm 0.70(\text{sys}) \text{ cpd}/100\text{t}$	$23 \pm 2 \text{ cpd}/100\text{t}$
^7Be ν	$22.67 \pm 17.77(\text{stat}) \text{ cpd}/100\text{t}$	$49 \pm 3 \text{ cpd}/100\text{t}$
pep ν	$2.66 \pm 1.04(\text{stat}) \pm 0.30(\text{sys}) \text{ cpd}/100\text{t}$	$2.1 \text{ cpd}/100\text{t}$

Table 5.1: Fit results for the light yield (LY) and event rates determined by spectral analysis of the selected experimental data sample with a free pep ν contingent. The given statistical error in the second column correspond to 68.27% confidence level. The expected rate for ^{11}C (without TFC cut), ^{210}Bi and ^7Be ν events in the last column are taken from the current ^7Be analysis presented in [32] whereas the expected pep ν rate is given in [8] including the LMA MSW solution.

The results of the fit is consistent with the expected signal at a 68.27% confidence level. In addition it is noticeable, that this fit does not have a deviation in the light yield similar to the fit on the MC data presented in section 4.1.3, which indicates, that the energy spectrum of ^{210}Bi calculated by the fitting procedure is in good agreement with the experimental data.

The fitted value for the ^7Be ν rate of $22.67 \pm 17.77(\text{stat}) \text{ cpd}/100\text{t}$ has a high statistical error and is far too low compared to the expected value of $49 \pm 3 \text{ cpd}/100\text{t}$. However, this was expected as its contribution is only observable in two bins of the energy spectrum (see figure 5.3), which makes the fit quite independent of this solar neutrino source.

The pep ν spectrum for this spectral analysis was determined with a fixed survival probability of $\langle P_{\nu_e \rightarrow \nu_e} \rangle = 0.3655$ calculated by J. N. Bahcall according to the LMA MSW solution [42]. The result of the fit is a pep neutrino rate of $2.66 \pm 1.04(\text{stat}) \pm 0.30(\text{sys}) \text{ cpd}/100\text{t}$, in agreement with the expectations. The statistical error is calculated for a 68.27% confidence level and the systematic error arises in the remaining external γ background at the FV of 1.8m (see section 5.2.1) assuming the worst case, that the distribution of the γ events equals the spectral shape of the pep neutrino signal.

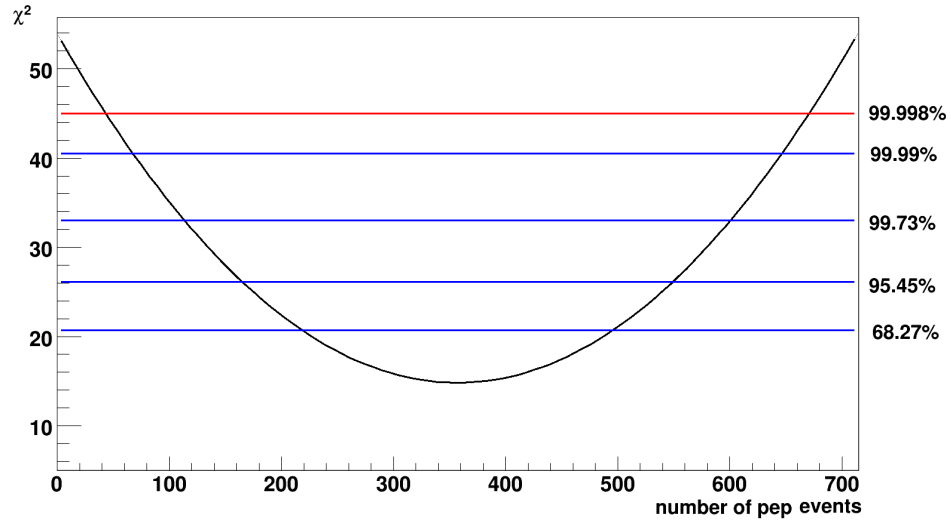


Figure 5.4: The description of the χ^2 distribution concerning the determined pep neutrino rate with a parabel fits perfectly well. The confidence level of a pep neutrino rate unequal to zero including the systematic error of this rate is shown in red.

Finally, including this systematic error, this fit provides a pep ν rate unequal to zero by 99.998% confidence level. This value was determined using the analysis method explained in section 3.5 on the χ^2 distribution of the fit concerning the pep neutrino event rate which is illustrated in figure 5.4. This χ^2 distribution was fitted with a parable leading to:

$$\chi^2(x) = 53.91 - 2.191 \cdot 10^{-1} \cdot x + 3.07 \cdot 10^{-4} \cdot x^2 \quad (5.2)$$

The errors of the determined parameters are in the order of a few per mill which shows, that the χ^2 distribution really has a parabolic shape. Even though it is not yet possible at the present status to claim the first real-time detection of solar pep neutrinos, this spectral analysis clearly proves the great capacity of BOREXINO for discovering this signal during the total life time of the experiment.

5.3 ^{40}K as possible Background Source for the pep Neutrinos

The primordial isotope ^{40}K has an abundance of 0.0117% and underlies the β^- decay (89.28%) with an endpoint at 1.311 MeV and the EC (10.72%) decay which emits γ radiation at 1.461 MeV. The percentage of the β^+ decay and the contribution of the electron neutrino of the EC are negligible. As the endpoint of the β^- decay is very close to the energy of the pep neutrinos, it could possibly provide a contribution to the pep ν signal determined in section 5.2. Therefore, it has to be taken into account in a combined spectral analysis, too. However, before this analysis was done, the fitting procedure for ^{40}K was first tested on MC data like for all other background and neutrino sources.

The β^- decay is a third unique forbidden transition and the calculation of the spectral shape requires an additional shape factor as presented in section 3.1.2. As this shape factor is not yet implemented in the BXMC, the *RDM* module was used for this crosscheck, treating the β^- as an allowed transition. The results of the spectral fit are illustrated in figure 5.5 and refer to the fit region between 100 p.e. and 520 p.e. In contrast to the ^{40}K β^- decay which was reproduced in agreement with the expectations, the γ peak calculated by the fitting procedure is not consistent with the MC data. The height and the width of the peak seem to be correct, but its position in the MC data is shifted to lower energies compared to the fit. This deviation has apparently its origin in the function for calculating the γ quenching which was introduced in section 3.4.1. A similar effect is visible in the fit of the ^{11}C spectra due to the two γ quanta from the electron-positron annihilation. Indeed it was seen in section 4.1.1, that the light yield resulting from the fit of the ^{11}C MC spectrum has the lowest value of all presented fits so far. This can qualitative be explained by the same difference in the γ quenching between the MC and the fitting procedure as it is observed for the ^{40}K isotope. However, this deviation is only present for fits on MC spectra. Regarding the fit of the experimental ^{11}C spectrum (see section 5.1) and the combined fit presented in section 5.2, the fitted light yield is in very good agreement with the expected value of $\sim 500 \frac{\text{p.e.}}{\text{MeV}}$. This indicates that the observed discrepancy will not be significant for the estimation of the ^{40}K rate based on experimental data.

The described deviation between the MC γ quenching and the γ quenching in the fitting procedure has been noticed also by other analysis groups in BOREXINO and is currently under investigation in the spectral fits as well as in the MC.

Including an additional free contingent of ^{40}K events to the radioactive sources considered in section 5.2, a new spectral analysis was performed on the same data sample used for the determination of the pep ν signal, neglecting screening effects for ^{210}Bi . Table 5.2 gives an overview on the fit results for the different parameters.

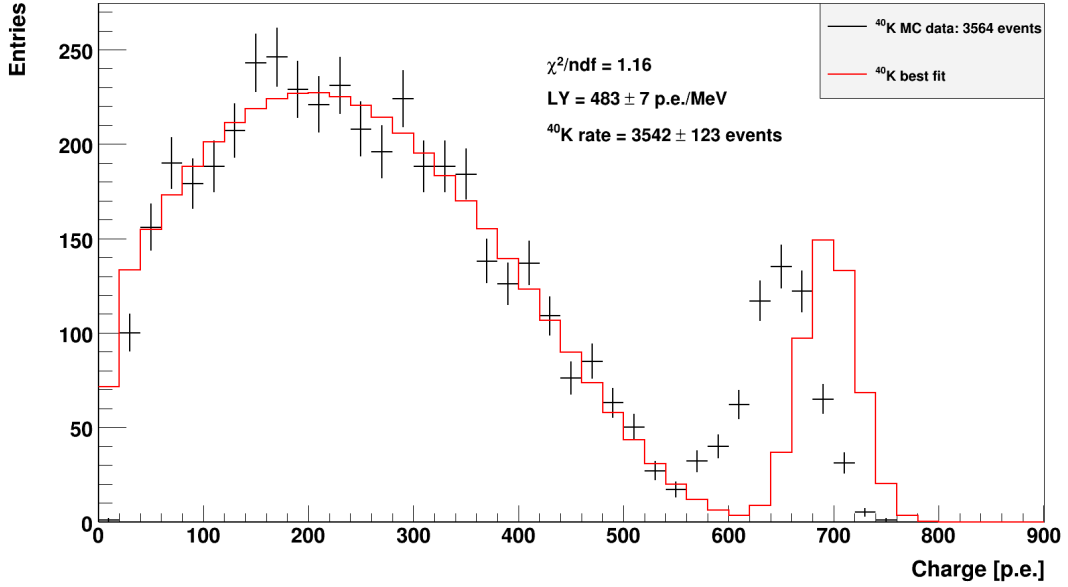


Figure 5.5: Spectral fit of a ^{40}K MC spectrum between 100 p.e. and 520 p.e. The energy spectrum of the β^- decay could be fitted with a satisfying result and in agreement with the expectations. However, the shift of the γ peak of the EC decay shows a discrepancy between the MC and the implemented γ quenching introduced in section 3.4.1.

The calculation of the spectral shape of ^{40}K was done considering the shape factor according to the forbidden transition in the β^- decay. Providing a ^{40}K event rate equal to zero, the fit returns the same values for all other considered sources. As this fit has one parameter more than before, the number of degrees of freedom is decreased by one which leads to a higher normalized χ^2 value of 1.059 and higher statistical errors.

On a 95% confidence level, the upper limit of the ^{40}K contribution within the experimental data can be estimated to 0.78 cpd/100t.

Parameter	Fitted value
LY	$503_{-13}^{+12}(\text{stat}) \frac{\text{p.e.}}{\text{MeV}}$
^{11}C	$2.75 \pm 0.42(\text{stat}) \text{ cpd}/100\text{t}$
^{210}Bi & CNO ν	$23.50 \pm 4.67(\text{stat}) \pm 0.70(\text{sys}) \text{ cpd}/100\text{t}$
^7Be ν	$22.67_{-19.42}^{+19.43}(\text{stat}) \text{ cpd}/100\text{t}$
pep ν	$2.66 \pm 1.13(\text{stat}) \pm 0.30(\text{sys}) \text{ cpd}/100\text{t}$
^{40}K	$0 \pm 0.57(\text{stat}) \text{ cpd}/100\text{t}$

Table 5.2: Fit results for the light yield (LY) and event rates determined by spectral analysis of the selected experimental data sample including a free ^{40}K contingent. The given statistical errors in the second column correspond to 68.27% confidence level. The fitted rate for ^{40}K events is equal to zero which leads to an upper limit for this decay of 0.78 cpd/100t at 95% confidence level.

Chapter 6

Summary of the results concerning spectral analysis in the BOREXINO experiment

In the context of this thesis a procedure for performing spectral analyses on BOREXINO data, was implemented (see chapter 3) and tested on Geant4 based Monte Carlo (MC) spectra (see chapter 4) before it was applied to experimental data (see chapter 5).

The fits on the MC data proved that the implemented procedure can reproduce the spectral shapes of β decay background and neutrino sources very well. Except for the MC data sample for ^{210}Bi events, simulated with the SCS (Special Cross Section) module, the determined values of the event rate and the light yield of the detector are always in agreement with the expectation. Particularly the spectral analysis of the MC data with pure pep ν contribution returns very good results. However, as mentioned, the fit of the MC data for the isotope ^{210}Bi , which was received from the BXMC SCS module taking into account the shape factor due to the forbidden transition of this nuclide, did not provide a satisfying value for the light yield. Furthermore the calculated spectral shape shows a deviation from the MC spectrum at energies below 100 p.e.

A second fit of a ^{210}Bi spectrum simulated with the RDM (Radioactive Decay) module, which treats the β^- decay of this isotope as an allowed transition, did not show any discrepancies when the spectral analysis was applied without the shape factor. Therefore, the reason for the observed deviation is a different implementation of the shape factor in the MC and the fitting procedure.

This topic is currently under investigation as it is not only significant for the analysis of pep neutrino events, but becomes even more important considering the search for solar CNO neutrinos.

A last successful test of the fitting procedure was performed on a BOREXINO data

sample of ^{11}C events which were tagged by the Three-Fold Coincidence (TFC) technique.

Afterwards a data sample including 633.82 d of detector life time was prepared for a spectral analysis with a free pep ν contingent. Muon cuts, a time cut to reject fast muon daughters, the identification of fast coincidences as well as the TFC method for tagging cosmogenic background were applied to eliminate the majority of background events. In addition, the FV was limited to 1.8 m which decreased the external γ background to 3.8% within the whole pep neutrino energy window. The spectral analysis performed on this selected data sample took into account the contribution of ^{11}C , ^{210}Bi , solar ^7Be neutrinos and pep neutrinos. The fit provides a pep neutrino event rate of $2.66 \pm 1.04(\text{stat}) \pm 0.30(\text{sys})$ cpd/100t in good agreement with the expected rate and includes a fixed survival probability of $\langle P_{\nu_e \rightarrow \nu_e} \rangle = 0.3655$ according to the MSW LMA solution. The statistical error was calculated for 68.27% confidence level whereas the systematic error arises in the remaining external γ background.

Finally, the statistical significance of the pep neutrino signal in this data sample could be determined to 99.998% confidence level.

In order to estimate the influence from the primordial radionuclide ^{40}K on the number of identified pep neutrino events, a second spectral analysis considering an additional contribution from ^{40}K decays was applied on the same data sample. This fit results in a ^{40}K event rate equal to zero within a 68.27% confidence level, which leads to an upper limit for this decay of 0.78 cpd/100t with 95% confidence level.

However promising the presented results are, a lot of additional work will have to be done in the future before the BOREXINO collaboration can claim the observation of solar pep neutrinos.

The combined fits which were applied to the experimental data sample neglect screening effects for ^{210}Bi . This results in a systematic error of 3% for the event rate of ^{210}Bi (see section 4.1.3). Therefore, a study of a possible correlation between the ^{210}Bi and pep neutrino event rate as well as the implementation of a better parameterization concerning the screening effects in the fitting procedure are important. Afterwards the combined fit has to be repeated to confirm the result on the determined pep neutrino signal by a more precise analysis.

Furthermore, a significant discrepancy concerning the γ quenching used for all spectral analyses and the Birks function implemented in the MC code has been found, which becomes significant in the case of ^{40}K . This topic has to be investigated to gain a better understanding of the detector's response. The calibration campaign with an external γ source done in July 2010 will provide the necessary data for this task.

In addition, the spectral analyses presented in this thesis might become more pre-

cise by using a different response function for the energy resolution of the detector, as the assumption of a gaussian distribution (see section 3.4.2) is the easiest model for the calculations.

Nevertheless, the spectral analysis performed in this work proves the great potential of BOREXINO for a first real-time measurement of solar pep neutrinos during the total life time of the experiment.

Chapter 7

Neutrino Oscillometry in LENA

Based on the positive experiences and the success of BOREXINO, the LENA experiment (Low Energy Neutrino Astronomy) was proposed as a next-generation liquid scintillator detector with a target mass of ~ 50 kt [48]. This project is currently in its design phase and at the time being a lot of effort is done towards the optimization of light detection and readout electronics, the determination of the properties of different liquid scintillators, the development of software tools for muon and electron tracking and event reconstruction and the study of background and neutrino events by Monte Carlo simulations. Together with MEMPHYS, a planned water Cherenkov detector of 500 kt target mass, and GLACIER, a 100 kt liquid argon time projection chamber, LENA forms the LAGUNA (Large Apparatus for Grand Unification and Neutrino Astrophysics) collaboration which studies the feasibility of a large-volume detector for observing low-energetic neutrinos and searching for the proton decay [49].

The first section summarizes the planned detector setup and gives a short overview on the physics program of LENA, before the idea of neutrino oscillometry is explained in detail. The last part of this chapter treats the application of spectral fits for separating the neutrino signal from the EC decay of ^{51}Cr , which is one possible source for a neutrino oscillometry experiment in LENA, from the background of solar ^7Be events.

7.1 The LENA Experiment

This section provides an overview on the LENA detector and its physics program. More detailed information on this topics can be found in the LENA Whitepaper [50] which will be published soon.

As shown in figure 7.1, the planned design of the LENA detector is very similar to BOREXINO. The target volume consisting of 50 kt is surrounded by a buffer liquid acting as a shielding against external radioactive background. Due to the limited

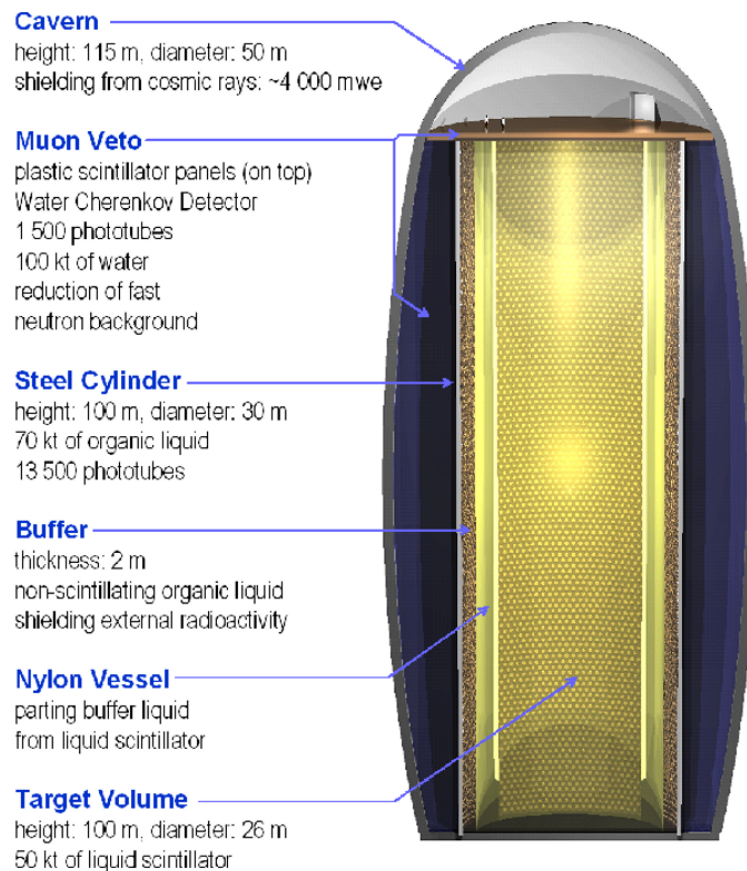


Figure 7.1: Schematic picture of the LENA detector. The detector design is similar to BOREXINO: The onion-like setup provides increasing radiopurity from the water Cherenkov detector outside to the target volume inside, which consists of 50 kt liquid scintillator. The given number of PMTs at the steel cylinder refers to PMTs with a diameter of 20 inch as used in Super-Kamiokande [27].

optical attenuation length of liquid scintillators, a cylindrical shape of 100m height with a radius of 13 m was chosen to minimize the distance from the center of the detector to the light detection system, which will be installed at the steel cylinder. The most promising candidates for the liquid scintillator so far are PXE ($C_{16}H_{18}$) and LAB ($C_{18}H_{30}$) which both have an attenuation length of more than 10 m at a wavelength of 430 nm.

Like BOREXINO, the LENA experiment will have an optical coverage of approximately 30%. This value can be achieved based on $\sim 50,000$ 8"-diameter PMTs equipped with light collectors. This will result in an effective detector light yield of $\sim 250 \frac{\text{p.e.}}{\text{MeV}}$.

The steel cylinder will be placed inside a water Cherenkov detector. This does not only provide an additional shielding against external radioactivity, but can also be used as active muon veto. In order to reduce cosmogenic backgrounds like ^{11}C , the depth requirement for the detector cavern is 4000 m.w.e. For this reason, the Center for Underground Physics in Pyhäsalmi (CUPP) in Finland and the Laboratoire Souterraine de Modane (LSM) in France are presently considered as the best sites for detector construction.

With its extraordinary target mass, the LENA detector will reach higher sensitivity and statistics than BOREXINO, provided that a similar level of radiopurity is achieved. Therefore, it will be possible to perform precision measurement of strong neutrino sources like the Sun as well as very rare event searches. In the following an extract from the physics program of LENA concerning neutrinos will be given:

- **Solar neutrinos:**

Depending on the energy threshold, the expected rate for solar pep and CNO neutrino events will be around 380 events per day and 600 events per day, respectively [51]. With approximately 5000 events per day from ^7Be recoils for a Fiducial Volume (FV) of 18kt, it will be possible to search for temporal variation in this rate that might for instance be caused by fluctuations in the temperature and density of the solar core.

- **Supernova neutrinos:**

The core-collapse explosion of a star with an initial mass of $8M_{\odot}$ at 10 kpc is expected to produce a signal of 10,000 to 15,000 neutrino events in LENA [35]. The total flux of the supernova neutrinos is measured via NC reactions, whereas CC reactions reveal the electron (anti-)neutrino flux.

- **Diffuse supernova neutrino background (DSNB):**

The DSNB originates from all core-collapse supernovae which took place within cosmic distances since the beginning of the universe. This faint neutrino flux will mainly be detected via the inverse β decay (see equation 2.2).

7.2 Neutrino Oscillometry with ^{51}Cr as monoenergetic neutrino source

Neutrino oscillometry is a new idea of measuring neutrino oscillation due to the unknown mixing angle θ_{13} proposed by J. D. Vergados and Yu. N. Novikov [52]. The basic idea of this method is, that instead of positioning the neutrino detector at the expected first oscillation maximum, the whole oscillation curve of the neutrino is observed. Therefore, a monoenergetic neutrino source of an extremely high activity, provided by isotopes that undergo the EC decay as there is only one neutrino in the final state (see section 3.1.1), is to be located at the top of the LENA detector. Assuming a sufficiently low neutrino energy (and therefore oscillation length) the change in the survival probability of the emitted electron neutrino could be monitored over the 100 m baseline of the detector.

The survival probability for this case can be derived from the ν_e disappearance oscillation probability [52] to

$$P_{\nu_e \rightarrow \nu_e}(L) \approx 1 - \sin^2(2\theta_{12}) \cdot \sin^2\left(\frac{\pi L}{33L_{23}}\right) - \sin^2(2\theta_{13}) \cdot \sin^2\left(\frac{\pi L}{L_{23}}\right) \quad (7.1)$$

under the assumption that $\delta m_{31}^2 \approx \delta m_{32}^2$. The corresponding oscillation length $L_{23} = \frac{4\pi E_\nu}{\delta m_{32}^2}$ can be approximated as $L_{23} [\text{m}] \approx E_\nu [\text{keV}]$. In this context, oscillations between the first and the second family can be neglected as they have a large oscillation length.

In order to obtain a sufficiently short baseline, an EC source with a neutrino energy in the region of 100 keV is preferable. However, such sources cannot be produced with a sufficient activity to exceed the natural radioactive background from ^{14}C in the scintillator.

Therefore, ^{51}Cr was investigated as a first possible source with a neutrino energy of 747 keV and a half live of $T_{\frac{1}{2}} = 28$ d. Such a source has already been produced with a very high activity and was used for the calibration of the GALLEX detector (see section 1.4) [53, 54].

As the the neutrino energy of this isotope lies close to the line of the solar ^7Be neutrinos, they provide the most important irreducible background to the signal of ^{51}Cr events in the detector.

The expected event rate R from the neutrino source can be calculated by

$$R = \rho_{e^-} \cdot \sigma(E_\nu, T) \cdot \frac{A(t)}{4\pi r^2} \cdot V(r) \cdot P_{\nu_e \rightarrow \nu_e}(E_\nu) \quad (7.2)$$

where ρ_{e^-} denotes the electron density for the considered liquid scintillator, $\sigma(E_\nu, T)$ stands for the neutrino-electron scattering cross section depending on the neutrino energy and the kinetic energy of the recoil electron, $V(r)$ is the observed target

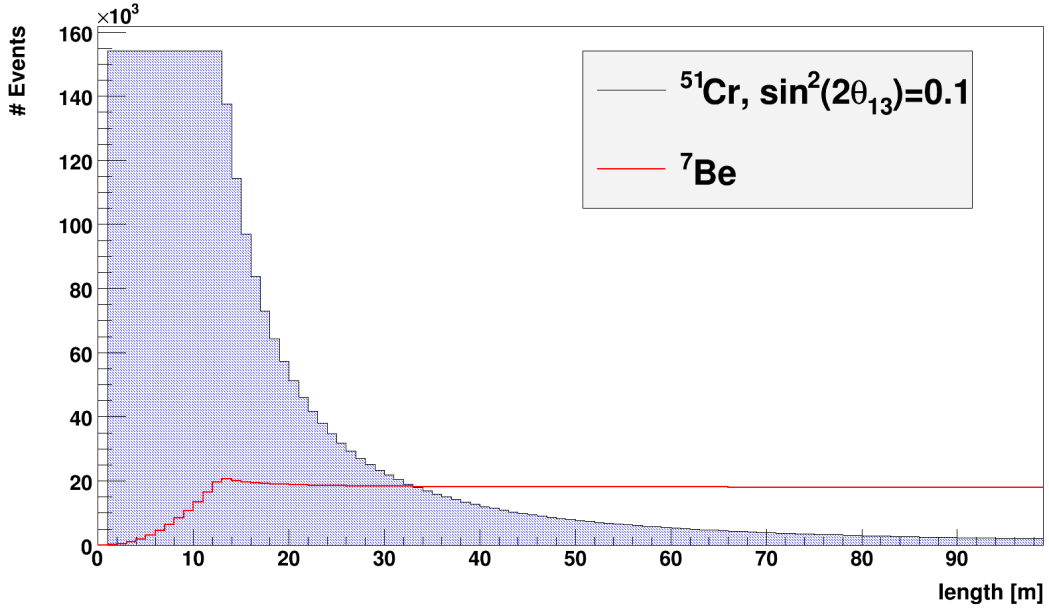


Figure 7.2: Dependence of the expected ^{51}Cr signal and the ^7Be background on the distance from the source. The ^{51}Cr signal dominates the ^7Be background only within the first 30 m of the detector.

volume at a distance r from the source and $A(t)$ denotes the source activity including the decrease of the activity during the duration t of the measurement due to the radioactive decay. In this most basic analysis the ^{51}Cr rate decreases with the squared distance ($\sim r^{-2}$), whereas the ^7Be background stays nearly constant. The dependence of the ^7Be and ^{51}Cr rates on the source distance is illustrated in figure 7.2. It shows, that the expected signal of the EC source exceeds the solar ^7Be neutrino rate up to a distance of 30 m. At distances of more than 50 m where the oscillation effect is expected to be visible, the ^{51}Cr rate is covered below the solar neutrino background.

Table 7.1 presents the results of a calculation for the expected rates of ^{51}Cr with an initial source activity of $7 \cdot 10^{17}$ Bq, which is currently considered as the maximum achievable activity of a chrome source produced by neutron irradiation in a nuclear reactor, LAB as liquid scintillator, a time period of 55 d and for different values of the mixing angle θ_{13} . The expected rates were determined for bins of 1 m width. The magnitude of the ^7Be neutrino signal was estimated by scaling the determined ^7Be rate of ~ 0.5 events per day and ton in BOREXINO [32] to the dimensions of LENA, assuming a homogeneous distribution in the target volume. As it can be seen in table 7.1 the detector was divided in two subvolumes. The first 12 m (near volume) are used as a normalization whereas the oscillation effects

detector region	first 12 m	last 88 m
$^{51}\text{Cr}, \sin^2(2\theta_{13}) = 0.1$	$1.91112 \cdot 10^6$	$1.43373 \cdot 10^6$
$^{51}\text{Cr}, \sin^2(2\theta_{13}) = 0.01$	$1.91126 \cdot 10^6$	$1.43632 \cdot 10^6$
$^{51}\text{Cr}, \sin^2(2\theta_{13}) = 0$	$1.91128 \cdot 10^6$	$1.43661 \cdot 10^6$
^7Be	$8.55924 \cdot 10^4$	$8.13421 \cdot 10^5$

Table 7.1: Expected rates for a ^{51}Cr source and solar ^7Be neutrinos for 55d of measurement. The event rate of ^{51}Cr was calculated for different values of $\sin^2(2\theta_{13})$. Even though the ^{51}Cr signal exceeds the number of ^7Be events significantly, the difference in the event rates between $\sin^2(2\theta_{13}) = 0.1$ and the no-oscillation hypothesis, is only 0.20% in the far volume of the detector.

are expected within the remaining 88 m of the detector (far volume). It should be noted, that the expected ^{51}Cr rate in the far volume for $\sin^2(2\theta_{13}) = 0.1$, which is close to the current experimental limit (see section 1.2), increases only by 0.20% compared to the no-oscillation hypothesis, which corresponds to a difference in the rate of 2880 events. This means, that the statistical error in the spectral analysis has to be considerably smaller to identify oscillations and to give improved limits on θ_{13} .

7.3 Sensitivity of the Spectral Fit on a ^{51}Cr signal with ^7Be Background

In the context of this thesis, the sensitivity of the spectral analysis introduced in chapter 3 on the separation of the ^{51}Cr signal from the solar ^7Be neutrino background is investigated.

Therefore a data sample consisting of electron recoil spectra from ^{51}Cr and ^7Be has been simulated. The basis of this calculation is the spectral shape described by formula 3.9, including the detector response as introduced in section 3.4 for an assumed light yield of $250 \frac{\text{p.e.}}{\text{MeV}}$.

Based on this model, MC spectra with rates of $1.43373 \cdot 10^6$ ^{51}Cr events and $8.13421 \cdot 10^5$ ^7Be events, assuming that $\sin^2(2\theta_{13}) = 0.1$ (see table 7.1), were

generated. The resulting MC data sample as well as the results of the spectral analysis are shown in figure 7.3. The three free parameters light yield, ^{51}Cr and ^7Be event rate were scanned in steps of $1 \frac{\text{p.e.}}{\text{MeV}}$ and 100 events, respectively. The normalized χ^2 value of this fit is very good and the determined event rates are close to the initial values. However, it was found that this spectral analysis preferred an upper constraint on the ^7Be rate. If this rate had not been limited to 813500 events, the result of the fit would be a high ^7Be and a low ^{51}Cr rate. This indicates, that the difference in the neutrino energy for both sources is too low to separate the two spectra with the current implementation of the spectral analysis for a light yield of $250 \frac{\text{p.e.}}{\text{MeV}}$.

The statistical error for the ^{51}Cr rate is only 0.26% of the fitted value. However, this is too high to distinguish the result of this fit from the no-oscillation hypothesis at a 68.27% confidence level.

As a consequence of the present results, if ^{51}Cr is chosen as neutrino source for the neutrino oscillation experiment, the rate would have to be extracted by statistical subtraction of the background. A spectral analysis would either require a different neutrino source (e.g. ^{75}Se) or an increase of the light yield that would improve the energy resolution of the detector. In addition, further studies of the sensitivity of the spectral fits on the different signals based on a realistic MC setup of LENA are needed.

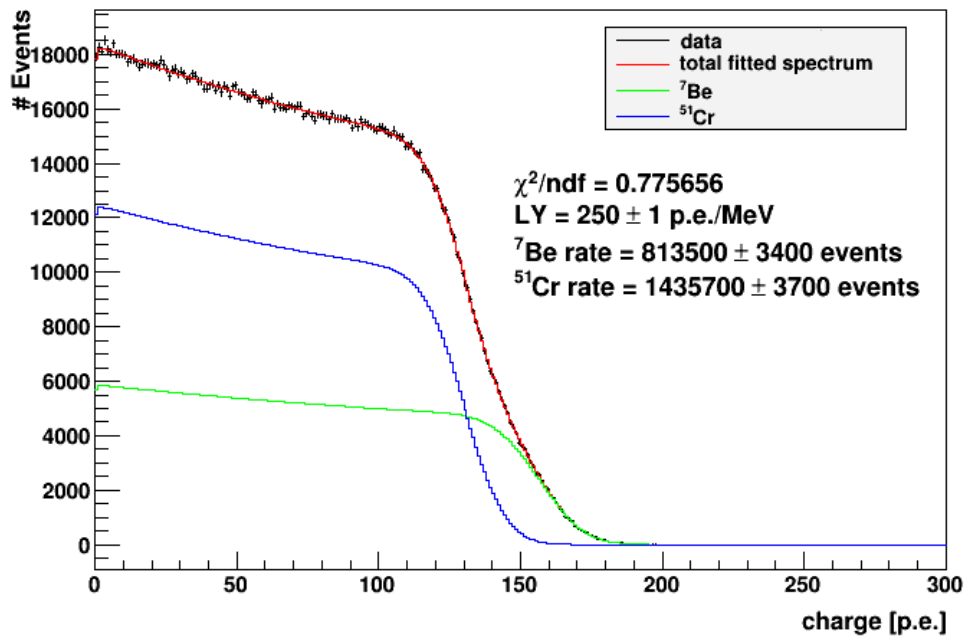


Figure 7.3: Combined fit on a simulated data sample of ${}^{51}\text{Cr}$ and ${}^7\text{Be}$ electron recoils. Although the fit returns excellent results with regard to the expected values for the light yield and the event rates, the fit accuracy on the event rate is not sufficient to distinguish the result from a no-oscillation hypothesis.

Chapter 8

Conclusion and Outlook

The solar neutrino experiment BOREXINO and the proposed next-generation experiment LENA are both based on a liquid scintillator technology. Solar neutrinos are detected indirectly via neutrino-electron scattering. The challenging task of separating these neutrino signals from background events within the data can only be performed by spectral analysis.

During this thesis, a procedure for performing this spectral analysis was developed, based on the theory of β decays and neutrino-electron scattering including the quenching effects and the energy resolution of the detector. It was tested on BOREXINO Monte Carlo data and on a ^{11}C spectrum of high purity, which was selected from experimental data by the Three-Fold Coincidence (TFC) technique. It was shown, that the spectral analysis works correctly on spectra from allowed β decays as well as on electron recoil spectra of neutrino events, reproducing the fitting parameters (light yield of the detector and the event rate) extremely well. In the context of this work, discrepancies between the Monte Carlo data and the spectra calculated by the fitting procedure could be observed. They concern the *SCS* (Special Cross Section) Monte Carlo module for the simulation of the forbidden β^- decay of ^{210}Bi and the γ quenching. Both topics are currently under investigation within the BOREXINO collaboration. The calibration campaign with an external γ source in July 2010, will hopefully answer the open questions on the γ quenching.

However, it has to be noted, that the spectral fit performed on the high purity ^{11}C spectrum extracted from the experimental data gave consistent results. This confirms the empirical function of the γ quenching used in this work.

After the tests of the spectral analysis on data samples with only one source contributing (radioactive nuclide or solar neutrino), a combined fit on an experimental data sample with 633.82 days of detector life time was performed with a free contingent of solar pep neutrino events, in addition to background signals from ^{11}C ,

^{210}Bi and events from solar ^7Be neutrinos. This fit returns a pep neutrino signal of $2.66 \pm 1.04(\text{stat}) \pm 0.30(\text{sys})$ cpd/100t, which is unequal to zero at a 99.998% confidence level. The numerical results for the different event rates do not change if the primordial isotope ^{40}K as additional background source is taken into account. However, the statistical significance of the pep signal is reduced to a 99.996% confidence level. This fit favours a ^{40}K rate equal to zero which sets an upper limit of 0.78 cpd/100t at 95% confidence level on the ^{40}K contribution in BOREXINO. Summarizing, it can be stated that the spectral analysis of the experimental data indicates the presence of the pep neutrino signal in the BOREXINO measurements.

However, as the present status of the work does not include screening effects for the β^- decay of ^{210}Bi due to insufficiencies of the based model, the search for a better parameterization concerning these effects and its implementation will be important for the future. Afterwards the combined spectral analysis to determine the pep neutrino rate has to be repeated to confirm the results of the first fit, which could not be done within the time limits of this thesis.

At the end of this work, neutrino oscillometry, a new technique which might be able to observe the still unknown neutrino mixing angle θ_{13} , was introduced. The measurement requires a very strong monoenergetic neutrino source. It was found that for a source consisting of ^{51}Cr with an initial activity of $7 \cdot 10^{17}$ Bq the effects due to neutrino mixing between the first and the third family result in a difference of 0.2% in the expected event rate of this source in the LENA detector. In this thesis, the sensitivity of the implemented spectral analysis to this signal was investigated. It was shown, that the statistical error for the ^{51}Cr event rate determined by the spectral fit is too high to distinguish between different oscillation models. Furthermore, the current implementation of the spectral analysis cannot separate the signal of the recoil electrons from the EC decay of ^{51}Cr from the events of the solar ^7Be neutrinos for an energy resolution of the detector based on a light yield of $250 \frac{\text{p.e.}}{\text{MeV}}$.

Concluding, it can be stated, that the developed tool for performing spectral analysis achieved good results concerning the data analysis in BOREXINO. The extension of the spectral fits by improving the calculation of the screening effects for β decays, the quenching effects for electrons and γ radiation and the response function for the energy resolution of the detector will provide a higher sensitivity in the detection of solar neutrinos in this experiment as it is already provided at the present status of the data analysis.

List of Figures

1.1	The pp fusion cycle.	8
1.2	The CNO fusion cycle.	8
1.3	The solar neutrino energy spectrum.	10
1.4	Predicted survival probability for solar neutrinos.	10
2.1	Design of the BOREXINO detector.	16
2.2	The Three-fold Coincidence technique.	21
2.3	BOREXINO energy spectrum.	23
2.4	First real time detection of ${}^7\text{Be}$ solar neutrinos by BOREXINO	24
2.5	Measurement of the survival probability for electron neutrinos. . . .	25
3.1	Energy distribution of the β decays for ${}^{11}\text{C}$ and ${}^{85}\text{Kr}$ with $F(Z, W) = 1$	29
3.2	Energy distribution of the β^- decay for ${}^{210}\text{Bi}$ and the effects of the shape factor.	30
3.3	Energy distribution of the β decays for ${}^{11}\text{C}$ and ${}^{85}\text{Kr}$ including the Fermi function.	32
3.4	Relative deviation between parameterization and an approximation of the Fermi function for ${}^{11}\text{C}$, ${}^{85}\text{Kr}$ and ${}^{210}\text{Bi}$	33
3.5	Electron recoil spectrum of the ${}^7\text{Be}$ solar neutrinos with 862 keV energy.	35
3.6	Electron recoil spectrum of the pep solar neutrinos with 1.442 MeV energy including energy resolution.	36
4.1	Spectral fit of the β^+ spectrum of ${}^{11}\text{C}$	41
4.2	Spectral fit of a β^- spectrum of ${}^{85}\text{Kr}$	41
4.3	Spectral fit of a β^- spectrum of ${}^{210}\text{Bi}$ including the shape factor. . .	43
4.4	Spectral fit of a β^- spectrum ${}^{210}\text{Bi}$ without shape factor.	43
4.5	Spectral fit of the electron recoil spectrum of solar ${}^7\text{Be}$ neutrinos. .	46
4.6	Spectral fit of the electron recoil spectrum of solar pep neutrinos. .	46

5.1	Spectral fit of a ^{11}C β^+ spectrum selected by TFC from BOREXINO data.	48
5.2	Radial distribution of selected events within the FV.	50
5.3	Combined fit of background and neutrino sources on experimental data with a free pep ν contingent.	51
5.4	The χ^2 parable concerning the determined pep neutrino rate.	53
5.5	Spectral fit of a ^{40}K MC spectrum.	55
7.1	Design of the LENA detector.	62
7.2	Dependence of the expected ^{51}Cr signal and the ^7Be background on the distance from the source.	65
7.3	Combined fit on a simulated data sample of ^{51}Cr and ^7Be electron recoils.	68

List of Tables

1.1	Elementary particles and gauge bosons in the Standard Model	2
1.2	Best values and limits for the oscillation parameters in vacuum	5
1.3	Solar neutrino fluxes and neutrino energies.	9
5.1	Fit results for the light yield and event rates determined by spectral analysis of the selected experimental data sample with a free pep ν contingent.	52
5.2	Fit results for the light yield and event rates determined by spectral analysis of the selected experimental data sample including a free 40K contingent.	56
7.1	Expected rates for a ^{51}Cr source and solar ^7Be neutrinos for 55 d of measurement.	66

Bibliography

- [1] K. Nakamura et al (Particle Data Group). Review on Particle Physics. *J. Phys. G*, 37(075021), 2010.
- [2] W. Pauli. *Collected Scientific Papers*, Volume 2. Interscience, 1964.
- [3] N. Schmitz. *Neutrino-physik*. Teubner-Studienbücher, Stuttgart, 1997.
- [4] S. P. Mikheyev and A. Y. Smirnov. Resonant Neutrino Oscillations in Matter. *Prog. Part. Nucl. Phys*, 23(p.41), 1989.
- [5] A. Halprin. Neutrino Oscillations in Nonuniform Matter. *Phys. Rev. D*, 34(p.3462), 1986.
- [6] L. Wolfenstein. Neutrino oscillations in matter. *Phys. Rev. D*, 17(p.2369), 1978.
- [7] J. N. Bahcall. *Neutrino Astrophysics*. University Press, Cambridge, 1989.
- [8] D. D'Angelo. *Towards the Detection of low energy Solar Neutrinos in BOREXino: Data Readout, Data Reconstruction and Background Identification*. Phd Thesis, Technische Universität München, 2006.
- [9] T. Lewke. Calibration and Efficiency Determination of the BOREXINO Muon Veto based on the First Realtime Measurements of ${}^7\text{Be}$ Solar Neutrinos. Diploma Thesis, Technische Universität München, 2007.
- [10] A. M. Serenelli J. N. Bahcall and S. Basu. 10,000 Standard Solar Models: A Monte Carlo Simulation. *Astrophys. J. Suppl*, 165(p.400), 2006.
- [11] J. N. Bahcall. Neutrino-Electron Scattering and Solar Neutrino Experiments. *Rev. Mod. Phys*, 59(p.2), 1987.
- [12] A. M. Serenelli J. N. Bahcall and S. Basu. New Solar Opacities, Abundances, Helioseismology and Neutrino Fluxes. *Astrophys. J.*, L85, 2005.

- [13] A. Friedland et al. Solar Neutrinos as Probes of Neutrino-Matter Interactions. *Physics Letters B*, 594(p.347), 2004.
- [14] J. N. Bahcall. The Luminosity Constraint on Solar Neutrino Fluxes. *Phys. Rev. C*, 65(025801), 2002.
- [15] T. Cleveland et al. Measurement of the Solar Electron Neutrino Flux with the Homestake Chlorine Detector. *Astrophys. J.*, 496(p.505), 1998.
- [16] GNO Collaboration. Complete Results for five years of GNO Solar Neutrino Observations. *Physics Letters B*, 616(p.174), 2005.
- [17] SAGE Collaboration. Solar Neutrino Flux Measurements by the Soviet-American Gallium Experiment (SAGE) for half the 22-year Solar Cycle. *J. Exp. Theor. Phys.*, 95(p.181), 2002.
- [18] Kamiokande Collaboration. Solar Neutrino Data covering Solar Cycle 22. *Phys. Rev. Lett.*, 77(p.1683), 1996.
- [19] Super-Kamiokande Collaboration. Atmospheric Neutrino Results from Super-Kamiokande and Kamiokande - Evidence for ν_μ Oscillations -. *Nucl. Phys. Proc. Suppl.*, 77(p.123), 1998.
- [20] Super-Kamiokande Collaboration. Solar Neutrino Results in Super-Kamiokande-III. *arXiv (hep-ex)*, 1010.0118, 2010.
- [21] SNO Collaboration. Low Energy Threshold Analysis of the Phase I and Phase II Data Sets of the Sudbury Neutrino Observatory. *Phys. Rev. C*, 81(055504), 2010.
- [22] KamLAND Collaboration. Production of Radioactive Isotopes through Cosmic Muon Spallation in KamLAND. *Phys. Rev. C*, 81(025807), 2010.
- [23] BOREXINO Collaboration. Science and Technology of BOREXINO: A real time Detector for low energy Solar Neutrinos. *Astropart. Phys.*, 16(p.205), 2002.
- [24] BOREXINO Collaboration. The BOREXINO Detector at the Laboratori Nazionali del Gran Sasso. *arXiv (physics.ins-det)*, 0806.2400v1, 2008.
- [25] M. Pallavicini. *Getting the first ${}^7\text{Be}$ ν Detection: Scintillator Purification, Detector Response and Data Analysis in BOREXINO*. Taup, 2007.
- [26] BOREXINO Collaboration. Light Propagation in a Large Volume Liquid Scintillator. *Nucl. Instrum. Meth. A*, 44(p.360), 2000.

- [27] M. Wurm. *Cosmic Background Discrimination for the rare Neutrino event search in BOREXINO and Lena*. Phd Thesis, Technische Universität München, 2009.
- [28] ROOT webpage. <http://root.cern.ch>, 28.11.2010.
- [29] BOREXINO Collaboration. Pulse-Shape Discrimination with the Counting Test Facility. *Nucl.Instrum.Meth.A*, 584(p.98), 2008.
- [30] Q. Meindl. Identification of Cosmogenic Background Signals in the Neutrino Experiment BOREXINO. Diploma Thesis, Technische Universität München, 2008.
- [31] BOREXINO Collaboration. First real time Detection of ${}^7\text{Be}$ Solar Neutrinos by BOREXINO. *Physics Letters B*, 658(p.101), 2008.
- [32] BOREXINO Collaboration. New Results on Solar Neutrino Fluxes from 192 days of BOREXINO Data. *Phys. Rev. Lett*, 101(091302), 2008.
- [33] BOREXINO Collaboration. Measurement of the Solar ${}^8\text{B}$ Neutrino Flux with 246 live days of BOREXINO and Observation of the MSW Vacuum-Matter Transition. *arXiv*, 0808.2868v3, 2010.
- [34] BOREXINO Collaboration. Observation of Geo-Neutrinos. *Physics Letters B*, 687(p.299), 2010.
- [35] J. M. A. Winter. Phenomenology of Supernova Neutrinos, Spatial Event Reconstruction, and Scintillation Light Yield Measurements for the liquid-scintillatordetector Lena. Diploma Thesis, Technische Universität München, 2007.
- [36] E. Fermi. Versuch einer Theorie der β Strahlen I. *Zeits. f. Physik*, 88(p.161), 1934.
- [37] K. Siegbahn. *Beta- and Gamma-Ray Spectroscopy*. North-Holland Publishing Company, Amsterdam, 1955.
- [38] A. Grau Carles. Beta Shapefactor Determinations by the Cutoff Energy Yield Method. *Nucl. Instrum .Meth. Phys. Res. A*, 551(p.312), 2005.
- [39] S. Zhang. *Computation of Special Functions*. John Wiley and Sons, New York, 1996.
- [40] B. Povh. *Teilchen und Kerne*. Springer Verlag, Berlin, Heidelberg, 2006.
- [41] A. Ianni. private communication.

- [42] J. N. Bahcall. Where do we stand with Solar Neutrino Oscillations? *Phys. Rev. D*, 58(096016), 1998.
- [43] G. 't Hooft. Prediction for Neutrino-Electron Cross-Sections in Weinberg's Model of weak interactions. *Phys. Lett. B*, 37(2), 1971.
- [44] J. B. Birks. Scintillations from Organic Crystals: Specific Fluorescence and Relative Response to Different Radiations. *Proc. Phys. Soc. A*, 64(p.874), 1951.
- [45] Wolfram Mathematica Online Integrator webpage. <http://integrals.wolfram.com>, 29.11.2010.
- [46] Geant4 webpage. <http://geant4.cern.ch/>, 28.11.2010.
- [47] Q. Meindl. private communication.
- [48] L. Oberauer, F. von Feilitzsch, W. Potzel. A large liquid scintillator detector for low-energy neutrino astronomy. *Nucl. Phys. B (Proc. Suppl.)*, 138(p.108), 2005.
- [49] D. Autiero et al. Large underground, liquid based detectors for astro-particle physics in Europe: scientific case and prospects. *JCAP*, 0711(011), 2007.
- [50] J. Beacom et al. A next-generation liquid-scintillator neutrino observatory, to be published.
- [51] S. Todor. Solar neutrinos with LENA and a spectroscopical analysis of liquid-scintillators. Diploma thesis, Technische Universität München, 2008.
- [52] Yu. N. Novikov J. D. Vergados. Exploring new features of neutrino oscillations with very low energy monoenergetic neutrinos. *Nucl. Phys B*, 839(p.1), 2010.
- [53] GALLEX collaboration. First results from the ^{51}Cr neutrino source experiment with the GALLEX detector. *Physics Letters B*, 342(p.440), 1995.
- [54] GALLEX collaboration. Final results of the ^{51}Cr neutrino source experiments in GALLEX. *Physics Letters B*, 420(p.114), 1998.

Acknowledgements

Zu allererst möchte ich mich bei Herrn Prof. Franz von Feilitzsch und Herrn Prof. Stefan Schönert bedanken, die mir diese Diplomarbeit ermöglichten und mich sehr freundlich am Lehrstuhl E15 aufgenommen haben.

Prof. Lothar Oberauer danke ich nicht nur dafür, dass er mir dieses außerordentlich interessante Diplomarbeitsthema gestellt hat, sondern auch für die vielen wertvollen Ratschläge, die er mir als Advisor während meiner Studienzeit gegeben hat.

Quirin Meindl gebührt mein Dank dafür, dass er mich in die Kunst der Datenanalyse eingewiesen hat und ich ihn während des gesamten Jahres mit Fragen zu diesem Thema löchern durfte. In diesem Zusammenhang sei erwähnt, dass er jedes meiner Ergebnisse mit kritischem Blick überprüft hat, was mich manches Mal fast hätte verzweifeln lassen. Aber gerade durch diese Skepsis habe ich sehr viel über das gründliche Arbeiten mit experimentellen Daten gelernt. Vielen Dank!

Michael Wurm danke ich für die hilfreichen Diskussionen, wenn ich bei meiner Arbeit mal nicht weiter wusste. Ob es der Neutrino Wirkungsquerschnitt, Detektoreigenschaften von BOREXINO und LENA oder ... waren, falls niemand eine Antwort wußte, hatte er eine parat, oder er brachte mich auf den richtigen Weg, um eine Lösung zu finden.

Bei meinen Bürokollegen Quirin Meindl, Jürgen Winter, Timo Lewke und Marc Tippmann bedanke ich mich für die äußerst angenehme Atmosphäre im Büro. Fast jeden Tag gut gelaunt, immer freundlich und hilfsbereit ... ihr seid einfach klasse! Ein weiteres Dankeschön geht an Quirin, Michael, Jürgen und Timo für das schnelle und effektive Korrekturlesen dieser Arbeit.

Allen anderen Mitgliedern vom Lehrstuhl E15, die ich nicht namentlich erwähnt habe, danke ich dafür, dass ich durch sie eine schöne Zeit an diesem Lehrstuhl hatte.

Der Mensch, dem ich zu größtem Dank verpflichtet bin, ist meine Mutter. Sie hat mich in jeder Lebenslage bedingungslos unterstützt und für mein Wohlergehen auf viel verzichtet. Ohne sie wäre mir dieses Studium nicht möglich gewesen.